Systems/Circuits

# Testing the Efficacy of Single-Cell Stimulation in Biasing Presubicular Head Direction Activity

**Stefano Coletta,[1,2] Markus Frey,[1] Khaled Nasr,[1,2] Patricia Preston-Ferrer,[1] and Andrea Burgalossi[1]**

[1]Werner-Reichardt Centre for Integrative Neuroscience, 72076 Tübingen, Germany and [2]Graduate Training Centre of Neuroscience, International Max Planck Research Schools, 72074 Tübingen, Germany

**To support navigation, the firing of head direction (HD) neurons must be tightly anchored to the external space. Indeed, inputs from external landmarks can rapidly reset the preferred direction of HD cells. Landmark stimuli have often been simulated as excitatory inputs from "visual cells" (encoding landmark information) to the HD attractor network; when excitatory visual inputs are sufficiently strong, preferred directions switch abruptly to the landmark location. In the present work, we tested whether mimicking such inputs via juxtacellular stimulation would be sufficient for shifting the tuning of individual presubicular HD cells recorded in passively rotated male rats. We recorded 81 HD cells in a cue-rich environment, and evoked spikes trains outside of their preferred direction (distance range, 11–178°). We found that HD tuning was remarkably resistant to activity manipulations. Even strong stimulations, which induced seconds-long spike trains, failed to induce a detectable shift in directional tuning. HD tuning curves before and after stimulation remained highly correlated, indicating that postsynaptic activation alone is insufficient for modifying HD output. Our data are thus consistent with the predicted stability of an HD attractor network when anchored to external landmarks. A small spiking bias at the stimulus direction could only be observed in a visually deprived environment in which both average firing rates and directional tuning were markedly reduced. Based on this evidence, we speculate that, when attractor dynamics become unstable (e.g., under disorientation), the output of HD neurons could be more efficiently controlled by strong biasing stimuli.**

*Key words:* **cortical physiology; head direction cell; *in vivo* electrophysiology; single-cell stimulation; spatial navigation**

**Significance Statement**

**The activity of head direction (HD) cells is thought to provide the mammalian brain with an internal sense of direction. To support navigation, the firing of HD neurons must be anchored to external landmarks, a process thought to be supported by associative plasticity within the HD system. Here, we investigated these plasticity mechanisms by juxtacellular stimulation of single HD neurons *in vivo* in awake rats. We found that HD coding is strongly resistant to external manipulations of spiking activity. Only in a visually deprived environment was juxtacellular stimulation able to induce a small activity bias in single presubicular neurons. We propose that juxtacellular stimulation can bias HD tuning only when competing anchoring inputs are reduced or not available.**

## Introduction

Navigation requires an internal compass that is thought to be provided by head direction (HD) cells, neurons that selectively increase their firing when the animal's head points in a specific direction. These neurons were originally discovered in the rat dorsal presubiculum (PreS) (Taube et al., 1990a,b), but later observed in other brain regions (for review, see Taube, 2007; Yoder and Taube, 2014). Most models have proposed that HD cells are linked together via excitatory and inhibitory connections to form an attractor network (McNaughton et al., 1991; Skaggs et al., 1995; Redish et al., 1996; Sharp et al., 1996; Zhang, 1996; Goodridge and Touretzky, 2000; Bicanski and Burgess, 2016; Simonnet et al.,

Received June 29, 2017; revised Jan. 15, 2018; accepted Feb. 5, 2018.

Author contributions: P.P.-F. edited the paper; P.P.-F. and A.B. designed research; S.C., M.F., P.P.-F., and A.B. performed research; S.C., M.F., and K.N. analyzed data; P.P.-F. and A.B. wrote the paper.

This work was supported by the Werner Reichardt Centre for Integrative Neuroscience (CIN) at the Eberhard Karls University of Tübingen [CIN is an Excellence Cluster funded by the Deutsche Forschungsgemeinschaft (DFG) within the framework of the Excellence Initiative EXC 307] and the DFG Grant BU 3126/1-1. We thank Alexandra Eritja for excellent technical assistance, Roxana Zeraati for contributing to data analysis, and Shimpei Ishiyama for illustrations.

The authors declare no competing financial interests.

M. Frey's present address: Kavli Institute for Systems Neuroscience, Centre for Neural Computation, Egil and Pauline Braathen and Fred Kavli Centre for Cortical Microcircuits, Norwegian University of Science and Technology, St. Olavs University Hospital, Trondheim, Norway.

Correspondence should be addressed to either Andrea Burgalossi or Patricia Preston-Ferrer, Werner-Reichardt Centre for Integrative Neuroscience, Otfried-Müller-str. 25, 72076 Tübingen, Germany, E-mail: andrea.burgalossi@cin.uni-tuebingen.de or patricia.preston@cin.uni-tuebingen.de.

DOI:10.1523/JNEUROSCI.1814-17.2018

 0270-6474/18/383287-16$15.00/0

2017) so that, when the animal moves its head, a "hill" of activity moves through a virtual ring. To serve as an internal sense of direction, such a compass needs to be reliably anchored to external landmarks; indeed, classical cue rotation experiments, in which a salient visual cue was rotated within the recording environment, have shown that HD cells are tightly "anchored" to external landmarks because their preferred directions are rapidly updated after cue rotation (Taube et al., 1990a; Goodridge and Taube, 1995; Taube and Burton, 1995; Taube, 1995a; Dudchenko et al., 1997; Goodridge et al., 1998; Golob and Taube, 1999). Associations with external landmarks can be learned very rapidly because a few minutes of exposure to a novel visual cue is already sufficient for gaining control over the HD system (Goodridge et al., 1998). The PreS (Clark et al., 2010; Yoder et al., 2011; Jacob et al., 2017), as well as the retrosplenial cortex, is thought to play a pivotal role in binding visual landmark information to the HD system. Anatomically, the PreS is the site of convergence of visual inputs from cortical areas (retrosplenial and primary visual cortex) and HD inputs from the dorsal thalamus (Vogt and Miller, 1983; Thompson and Robertson, 1987; van Groen and Wyss, 1990a,b; Shibata, 1993; Huang et al., 2017). Moreover, lesion studies have shown that, after PreS inactivation, thalamic HD cells are substantially less influenced by external landmarks (Goodridge and Taube, 1997), indicating that the PreS plays a key role in allowing visual landmarks to exert control over the HD system.

Landmark control of HD firing has been modeled as a dynamic (and plastic) feedforward interaction between "visual cells" (encoding landmark information) and HD neurons. Specifically, landmark stimuli have often been simulated as excitatory inputs from visual cells to the HD attractor network; when such inputs are sufficiently powerful, preferred directions switch abruptly to the landmark location (Blackstad, 1956; Knierim et al., 1995; Goodridge et al., 1998; Song and Wang, 2005; Knight et al., 2014; Page et al., 2014; Jeffery et al., 2016). Confirming these predictions, recent work in the *Drosophila* ellipsoid body has indeed shown that attractor dynamics can be rapidly modified by optogenetic stimulation of direction-sensitive neurons outside of the activity hill (Kim et al., 2017). The inputs from visual cells onto HD neurons are postulated to become strengthened (in a Hebbian-like manner) as a result of learning; therefore, postsynaptic spiking might be necessary for increasing the weights of landmark inputs (Skaggs et al., 1995).

In the present work, we tested whether evoking postsynaptic spikes in individual PreS HD neurons could be sufficient for engaging cell-autonomous plasticity mechanisms and thus modifying HD tuning. We took advantage of a recently established head-fixed preparation (Preston-Ferrer et al., 2016) for juxtacellularly recording and stimulating single PreS neurons in passively rotated rats. We show that, in a cue-rich environment, the HD tuning of individual neurons remains stable despite strong activity manipulations outside of the preferred direction. We provide initial evidence that, in a sensory-deprived environment, in which the HD tuning and average firing rates of PreS neurons are markedly reduced, juxtacellular stimulation can induce a small but significant spiking bias at the stimulus direction.

## Materials and Methods

*Juxtacellular recordings.* All experimental procedures were performed according to German guidelines on animal welfare under the supervision of local ethics committees. Experimental procedures for obtaining juxtacellular recordings, signal acquisition and processing, and animal tracking in awake, head-fixed male Wistar rats were performed as described previously (Preston-Ferrer et al., 2016). Briefly, glass pipettes with resistance 4–6 MΩ were filled with standard Ringer's solution containing the following (in mM): 135 NaCl, 5.4 KCl, 5 HEPES, 1.8 $CaCl_2$, and 1 $MgCl_2$, pH 7.2. In a subset of recordings, Neurobiotin (1.5–3%; Vector Laboratories) or Biocytin (1.5–3%; Sigma-Aldrich) was added to the electrode solution. Osmolarity was adjusted to 290–320 mOsm.

We used head-restraint and passive rotation procedures following our previous study (Preston-Ferrer et al., 2016; see details in "Experimental design" section). For these experiments, animals were pre-implanted with a metal post and a recording chamber under ketamine/xylazine anesthesia. After surgery, animals were housed individually on a 12 h light/dark schedule. Food and water were available *ad libitum*. After a recovery period, animals were slowly habituated to head fixation and to the rotation apparatus under slightly dimmed ambient illumination in the cue-rich environment of the laboratory setting (referred as the "Open configuration"). Craniotomies ($<1$ mm$^2$) were performed at the same coordinates (0–0.5 mm posterior and 3–3.7 mm lateral from lambda), as in Preston-Ferrer et al. (2016) because they have proven to be reliable for targeting with high accuracy the dorsal portion of the rat PreS. Before juxtacellular recordings, mapping experiments with low-resistance (0.5–1 MΩ) pipettes were routinely performed to estimate the location of the PreS precisely. Targeting was based on characteristic electrophysiological signatures of the PreS (Preston-Ferrer et al., 2016) and neighboring structures. Specifically, electrode penetrations in the subiculum served as a clear anatomical landmark for precisely estimating the anterior border of the dorsal PreS due to the characteristic high-firing rates, burstiness, and lack of HD activity of the principal subicular units. Moreover, the transition from the angular bundle into the PreS, as well as the location of PreS layer 2 (Preston-Ferrer et al., 2016), could be estimated precisely based on the associated increases in multiunit spiking activity. The reliability of our targeting procedures, validated in our previous work (Preston-Ferrer et al., 2016), were further confirmed in the present study by anatomical verification of the recording sites and/or recovery of juxtacellularly labeled neurons (see "Anatomical verification of recording locations" section).

Single-cell stimulations were performed as described previously (Diamantaki et al., 2016) by injecting brief pulses (1–3 ms) of positive current (range 10–50 nA) while the animal's head was held stationary, facing away from the neuron's preferred direction. Our stimulation procedures (as in Diamantaki et al., 2016) provided transient access to the cell membrane potential, thereby inducing a rapid increase in spiking activity above baseline firing rates. After successful stimulation, membrane resealing typically occurred within a few seconds after stimulation, which resulted in rapid cessation of evoked firing. In a minority of cases, small amounts of negative current (~1–5 nA) were injected to promote the resealing process. Long evoked spike trains (>10 s) were also included in the analysis (Fig. 2*D* and Fig. 2-2, available at https://doi.org/10.1523/JNEUROSCI.1814-17.2018.f2-2) because these long, depolarization-induced trains resembled the "persistent-like" activity patterns of HD neurons. On average, our stimulation procedures led to very similar increases in spiking activity above baseline firing rates in the stimulation dataset in the Open (STIM-Open) (Fig. 2*D* and Fig. 2-2, available at https://doi.org/10.1523/JNEUROSCI.1814-17.2018.f2-2) and stimulation dataset in the Closed (STIM-Closed) configuration. (See Fig. 6*E* and Fig. 2-2, available at https://doi.org/10.1523/JNEUROSCI.1814-17.2018.f2-2). In both datasets, multiple stimulations were performed in a subset of neurons (STIM-Open dataset, $n = 130$ stimulations in 81 neurons; STIM-Closed dataset, $n = 42$ stimulations in 25 neurons). The locations of the additional stimulations were close to the location of the first one (median distance from first stimulation: STIM-Closed dataset, 2.6°; STIM-Open dataset, 5.9°). In the no stimulation (No-STIM) dataset, additional "no stimulations" (35 'no-stimulations' in 25 neurons) were performed in a subset of neurons at a close distance from the first "no stimulus" direction (median distance from first "no-stimulation," 2.7°). In these neurons, data from multiple stimulations were pooled for the analysis (see details in the "Analysis of electrophysiology data" section below).

Juxtacellular labeling was performed by using standard labeling protocols (Pinault, 1994, 1996) and modified procedures, which consisted in rapidly breaking the dielectric membrane resistance by short (1–3 ms), "buzz-like" current pulses, which provided rapid access to cell entrainment by juxtacellular current injection (i.e., 200 ms square current pulses; Pinault, 1994). After cell labeling, animals were either immediately perfused for anatomical analysis or returned to their home cage and perfused ~2–4 h after labeling. Juxtacelluar labeling was performed on the last penetration of the last recording session with the aim of gaining additional confirmation of the targeting procedures. Indeed, all identified neurons ($n = 11$) were recovered in PreS. However, only two neurons contributed to the stimulation datasets; therefore, possible structure–function relationships between stimulation effects and cell identity/laminar location cannot be resolved. The juxtacellular voltage signal was acquired via an ELC-03XS amplifier (NPI Electronic), sampled at 20 kHz by a POWER1401–3 data-acquisition interface (CED) under the control of Spike2 version 8.02 software. The orientation of the rat's head was tracked using a LED placed on the back of the turntable consistent with the sagittal plane of the animal. Animal tracking was performed by acquiring a video (25 Hz frame rate) with IC Capture Software (The Imaging Source).

*Experimental design*. The rotation apparatus (Preston-Ferrer et al., 2016) consisted of a Plexiglas rat chamber (20 × 8 cm, with 4-cm-high transparent walls) fixed on a stainless-steel plate (40 × 30 cm). This plate could rotate via a central pin relative to a stainless-steel bottom base. Rotations were performed manually by the experimenter.

In the Open configuration, the rats had visual access to proximal cues available in the immediate vicinity (e.g., computer screens, cold-light source, stereomicroscope) and distal cues (i.e., Faraday cage, ceiling, curtains) (see also Preston-Ferrer et al., 2016). These cues were thus the most likely source of "anchoring" stability to HD firing (for review, see Knierim et al., 1995).

The Closed configuration consisted of a cylinder placed around the rotating platform. The cylinder (diameter: 35 cm, height: 50 cm) was custom-built out of aluminum and the inside was covered in dark black paper to avoid reflections of the LED on the aluminum surface. To prevent access to distal cues, recordings were performed in the dark and the top of the cylinder was closed in most recordings. In this configuration, the major polarizing cue was a white LED placed at a distance of ~10 cm from the rat's head.

For the subset of experiments in which neurons were stimulated in the Open configuration ($n = 81$; see Fig. 2), the following protocol was used: after obtaining a recording from a HD cell in the Open configuration and assessing its preferred firing direction by online (audio/visual) monitoring of spiking activity, the head of the rat was kept stationary and facing away from the preferred direction and the cell was fired by juxtacellular current injection (see "Juxtacellular recordings" section above). After stimulation, the spiking activity of the neuron was monitored during passive rotations (experimental protocol schematically shown in Fig. 2*A–C*).

For the subset of experiments in which neurons were sequentially recorded in the Open and Closed configurations ($n = 69$; see Fig. 3), the activity of the same neurons was first monitored in the Open configuration and the cylinder was then lowered around the animal, the lights were switched off, and a single white LED was turned on. After this, the spiking activity of the same neuron was monitored during passive rotations (experimental protocol schematically shown in Fig. 3*A*, *B*). For a subset of neurons, the activity was further recorded in an additional Open session (Open_2, $n = 23$; Fig. 3*C*).

For the subset of experiments in which neurons were stimulated in the Closed configuration ($n = 25$; see Fig. 6), HD activity was monitored as described above for the Open–Closed dataset. After recording in the Closed configuration, neurons were fired outside of their preferred direction (if one preferred direction could be assessed online; e.g., Fig. 6*A–D*) or at a random direction (if no clear preferred direction could be established). The same logic was applied to the No-STIM controls. After stimulation, the spiking activity of the neuron was monitored during passive rotations (experimental protocol schematically shown in Fig. 6*A–D*). The same procedures were applied to the No-STIM dataset ($n = 25$), with the only difference that cells were not fired by current injection in the Closed configuration, but the head of the rat was just kept stationary at the No-STIM direction without juxtacellular stimulation being performed.

For cue rotation experiments ($n = 11$; see Fig. 5), neurons were not recorded in the Open configuration, but juxtacellular recordings were established directly in the Closed configuration. This was necessary due to the low abundance of neurons that retained significant directional modulation in the Closed configuration; nondirectional neurons were discarded, whereas HD cells were recorded and tested as shown in Figure 5*A*. In these experiments, a second identical visual cue (LED2) was placed 90° away from LED1 (Fig. 5*A*). The activity of the same neuron was monitored during the transitions LED1→LED2 and LED2→LED1, corresponding to 90° cue rotations (experimental protocol schematically shown in Fig. 5*A*). Cue rotation sessions were interleaved with brief dark phases (Fig. 5*B*); these dark periods in which the LEDs were turned off were deemed as necessary for disorienting the animals, although this assumption was not tested explicitly in the present work.

Sample sizes were estimated on the basis of previously published data using *in vivo* single-cell stimulation (Houweling et al., 2008; Lee et al., 2012; Bittner et al., 2015; Diamantaki et al., 2016). Thirty male Wistar rats were used for awake experiments: 26 for the STIM-Open, STIM-Closed, and No-STIM datasets (Table 1 and Table 1-1, available at https://doi.org/10.1523/JNEUROSCI.1814-17.2018.t1-1) and four for the cue rotation experiments (Fig. 5). Animals were recorded chronically over the course of several days (typically 1–5 d) and contributed data points to more than one dataset (see details in Table 1-1, available at https://doi.org/10.1523/JNEUROSCI.1814-17.2018.t1-1).

*Extracellular recordings and visual stimulation*. Male Wistar rats ($n = 4$) were anesthetized with a combination of urethane and ketamine (Quilichini et al., 2010; Beed et al., 2013) and head-fixed on a stereotaxic apparatus. Surgery and recordings were performed as described previously (Beed et al., 2013). Multiunit spiking activity was recorded via tungsten electrodes (0.5 MΩ; World Precision Instruments). Extracellular signals were acquired via an EXT-HS-M amplifier (NPI Electronic) and band-pass signals (100 Hz, 5 kHz) were acquired by filtering the extracellular signals via a DPA-2F2 filter unit (NPI Electronic). Electrodes were targeted to the dorsal PreS using the same targeting procedures as described in the "Juxtacellular recordings" section above. Light-flash stimuli (2 s duration) were delivered by means of a white LED positioned at ~10 cm to the contralateral eye controlled by the POWER1401–3 data-acquisition interface (CED) and the Spike2 version 8.02 software.

*Immunohistochemistry and neuronal reconstruction*. For histological processing, animals were killed with an overdose of pentobarbital and perfused transcardially with 0.1 M PBS followed by a 4% paraformaldehyde solution. Brains were cut on vibratome to obtain 70-μm-thick parasagittal sections. To reveal the morphology of juxtacellularly labeled cells (i.e., filled with neurobiotin or biocytin), brain slices were processed with streptavidin-546 (Life Technologies) as described previously (Tang et al., 2014). Immunohistochemical stainings for Calbindin (monoclonal or rabbit anti-Calbindin D28k, 1:2000; Swant) and NeuN (anti-NeuN A60, 1:1000; Millipore) were performed as described previously on free-floating sections (Ray et al., 2014). Fluorescent images were acquired by epifluorescence microscopy (Axio imager; Zeiss). After fluorescence images were acquired, the neurobiotin/biocytin staining was converted into a dark DAB reaction product. Some sections underwent an $Ni^{2+}$-DAB enhancement protocol (Klausberger et al., 2003). Neuronal reconstructions were performed manually on DAB-converted specimens with Neurolucida software (MBF Bioscience) and displayed as 2D projections. Long-range axonal projections of the cell in Figure 1*B* were truncated for display purposes.

*Anatomical verification of the recording locations*. In half of the brains (13 of 26), the recording locations were verified by histological analysis. For aiding the identification of tracks, in a subset of cases, juxtacellular labeling was performed (8 of 26; see details in Results). In few cases ($n = 2$), a spillover of biocytin in a single location or along the electrode track (as in Fig. 1*D*) was performed. Brains were cut on a vibratome to obtain 70-μm-thick parasagittal sections and further processed for NeuN immunohistochemistry and/or biocytin labeling (as indicated in the

"Immunohistochemistry and neuronal reconstruction" section) or processed for cytochrome oxidase activity (according to standard protocols; Naumann et al., 2012). The majority of electrode tracks were visible from immunisthochemical or histochemical preparation (120 of 149) and were reconstructed manually on a reference anatomical frame of the dorsal PreS (medial, intermediate, and lateral extent; see also Preston-Ferrer et al., 2016). A minority of tracks were recovered from the subiculum (5 of 120) and none in the retrosplenial cortex; although very unlikely (see Results for details), the possibility that a minority of HD cell recordings might originate from neighboring strucutures (e.g., retrosplenial cortex and subiculum) cannot be formally ruled out.

For the visual stimulation experiments, the location of the recording sites was confirmed by aligning tungsten electrode tracks to anatomically verified electrolytic lesions ($n = 6$), as described previously (Beed et al., 2013). The location of all recordings included in the analysis ($n = 14$) was assigned to the PreS. We note, however, that the relatively large lesions (e.g., Fig. 4*B*) prevented precise and rigorous layer assignment of the recording sites.

*Analysis of electrophysiology data and statistical analysis.* Spike signals from juxtacellular traces were isolated by sorting spikes manually with the help of principal component analysis, as described previously (Burgalossi et al., 2011). For extracellular recordings (visual stimulation experiments in Fig. 4), large-amplitude spike signals above the noise level were isolated manually from the high-pass-filtered traces. Because spikes were larger than the noise level, but often too small to be individually sorted, they are referred to as "multiunit activity" herein. A single white LED positioned on the rotating platform was used for extracting the HD angle and the angular velocity. The angular velocity was calculated based on smoothed *X* and *Y* coordinates of the tracking (averaged across a 600 ms rectangular sliding window). An angular velocity cutoff (0.1 rad/s) was applied for isolating periods of rest from rotational movement and only spikes during movement were included in further analysis. Recordings (or portions of recordings) were cellular damage was observed in the electrophysiology were excluded from the analysis (as in Pinault, 1996; Herfst et al., 2012). Putative fast-spiking interneurons ($n = 11$) were classified according to spike shape and firing rate criteria (as in Preston-Ferrer et al., 2016). These criteria were confirmed by cell identification in our previous study (Preston-Ferrer et al., 2016).

To quantify HD tuning, we constructed HD tuning curves by dividing the number of spikes by the occupancy for each HD bin (36 bins; half smoothing window = 25°). Preferred directions were estimated as the direction of the average Rayleigh vector. The HD index of a cell was defined as the average Rayleigh vector over all bins, as described previously (Boccara et al., 2010; Tukker et al., 2015). A neuron was defined as an HD cell if its HD index was >0.3 and its spiking activity was significantly modulated by HD ($p < 0.05$; Rayleigh test; Berens, 2009). Only cells that met the HD criteria in the Open configuration were included in the present study (with the exception of recordings that were established directly in the Closed configuration; see description of cue rotation experiments in "Experimental design" section). For the cue rotation experiments (Fig. 5), neurons were included in the analysis if their firing activity was significantly modulated by HD under the LED1 and LED2 conditions (Fig. 5*A*); a criterion of HD index >0.3 was not applied here due to the reduced HD tuning in the Closed configuration (Fig. 3).

Analysis of stimulation effects (Q ratios) was performed on unsmoothed tuning curves. For cells that were stimulated multiple times (see description of single-cell stimulations above), the tuning curves for the intervals after each stimulation were aligned at their respective stimulus directions and averaged. The same was done for the tuning curves before stimulation. This produced a single pair of prestimulation and poststimulation tuning curves for each cell. The results of the present study do not depend on the pooling procedures because performing the analysis (as in Figs. 2*I*, 6*G*) on the individual stimulations leads to qualitatively similar results and does not alter the statistical significance of our findings ($p = 0.67$ and $p = 0.00085$, respectively). The same holds true for the No-STIM dataset ($p = 0.41$ if the analysis is based on the individual no stimulations). To quantify the effect of single-cell stimulation on the HD tuning of a cell, tuning curves were used to compute the ratio between the average firing rate within ($FR_{in}$) and outside ($FR_{out}$) of a 30° interval centered on the stimulus direction ($Q = FR_{in}/FR_{out}$). The modulation index was defined as follows: (Q after STIM − Q before STIM)/(Q after STIM + Q before STIM). The center of mass (COM) of HD tuning curves was calculated as the geometric centroid of the averaged and normalized tuning curves (the tuning curves were aligned to their respective stimulus directions before averaging). The statistical significance of the observed changes in modulation index and COM shift was assessed by a label-shuffling test. For assessing random variability of firing in the Closed configuration, for each STIM (or No-STIM) recording in the Closed configuration ($n = 50$ neurons), individual recording epochs before or after individual STIM (or No-STIM) were randomly assigned the labels "before stimulation" or "after stimulation." For each permutation, a modulation index and an average COM shift were computed and *p*-values were calculated from the resulting null distributions (1000 shuffles). The spike-time shuffling test was performed by randomly time-shifting the spike sequence of each recording, as described previously (Preston-Ferrer et al., 2016).

For visual stimulation experiments (Fig. 4), only neurons with >10 individual stimulation trials were included in the analysis. Firing rate modulation by visual stimulation (Fig. 4*D*) was assessed by calculating the average firing rate 0.5 s before stimulation and 0.5 s after stimulation for all trials. Latency of visual responses was calculated as in Gawne et al. (1996). Briefly, latencies were defined from peristimulus time histograms (5 ms bin size, smoothing window = 25 ms) as the time between stimulus onset and the half-peak of the response. Latencies were calculated only for the subset of neurons ($n = 9$) in which the peak response was at least twice the baseline firing rate to avoid the variability arising from calculating latencies for very weak visual responses (as in Gawne et al., 1996).

Statistical significance was assessed by a two-sided Wilcoxon rank-sum test (for unpaired data) or Wilcoxon signed-rank test (for paired data) with 95% confidence intervals (Bonferroni correction for multiple comparisons). Data are presented as mean ± SD unless stated otherwise.

## Results

### Recording presubicular HD cells in passively rotated, head-fixed rats

In the present study, we took advantage of a recently established head-fixed preparation for recording HD cells in the dorsal portion of the rat PreS (Fig. 1*A*; Preston-Ferrer et al., 2016). Individual PreS neurons were blindly sampled by juxtacellular procedures and their head directionality was assessed by manually performing alternate clockwise and counterclockwise rotations (Preston-Ferrer et al., 2016). As in previous single-cell stimulation work (Houweling et al., 2010; Doron et al., 2014; Diamantaki et al., 2016), routine cell identification and/or assignment of recording sites could not be achieved because multiple recordings and electrode penetrations prevented unequivocal identification of the recording locations. However, for the reasons outlined below, we believe that our recordings stem from the dorsal portion of the PreS.

First, before recording, coordinate-based targeting was always complemented by mapping experiments (see details in Materials and Methods) for precisely localizing the dorsal PreS. Characteristic local field potential signatures (Preston-Ferrer et al., 2016), together with the large abundance of HD neurons, served as reliable features for localizing the dorsal PreS. The reliability of this mapping strategy was confirmed in our previous study (Preston-Ferrer et al., 2016), in which all identified HD cells ($n = 27$) were recovered in the PreS and none in the neighboring subiculum or retrosplenial cortex.

Second, despite the above considerations, in a subset of animals (eight of 26; Table 1-1, available at https://doi.org/10.1523/JNEUROSCI.1814-17.2018.t1-1), we verified the anatomical location of our recordings by juxtacellular labeling. A representative example is shown in Figure 1*B*. This HD cell was identified

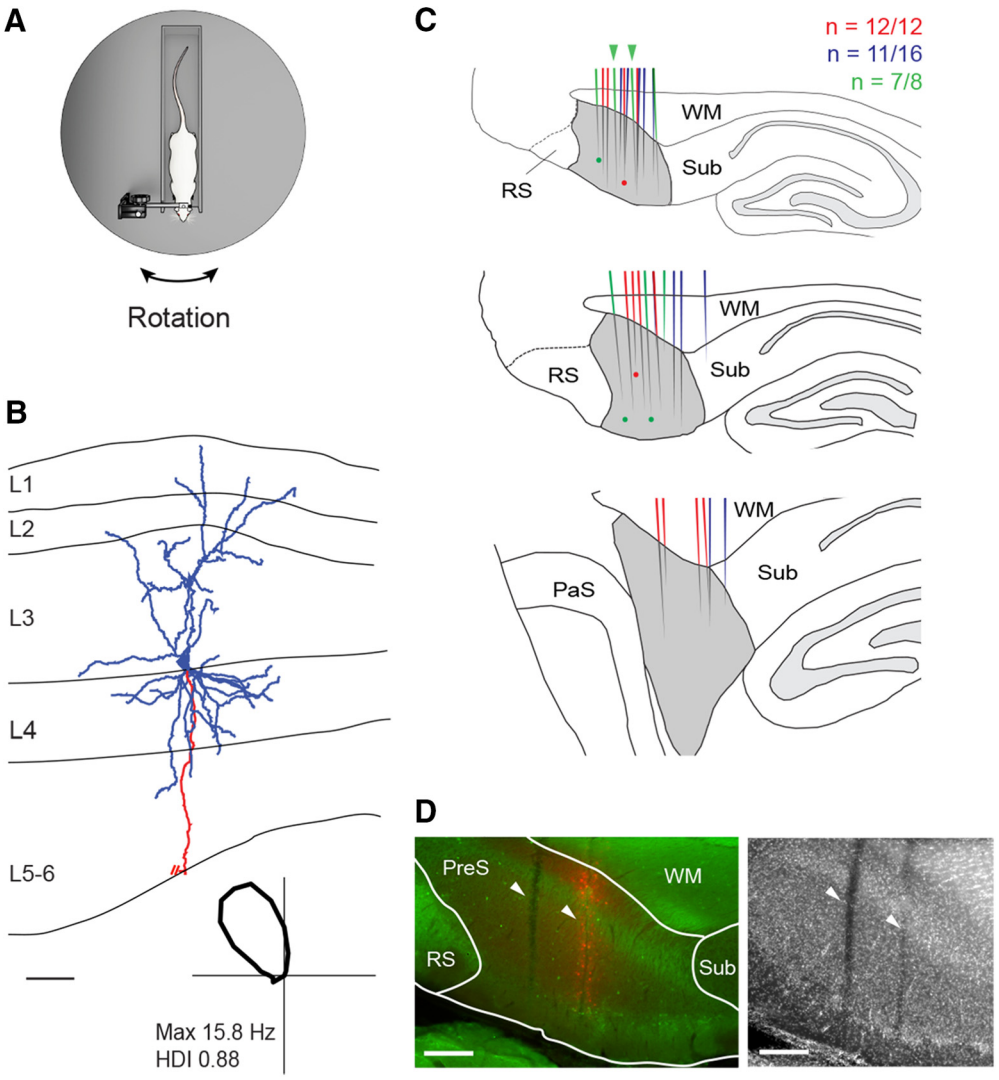


**Figure 1.** Juxtacellular recordings of presubicular HD neurons in head-fixed rats. ***A***, Schematic representation of the Open recording configuration, consisting of a head-fixed rat on a rotating platform in the presence of a rich set of proximal and distal cues (see also Preston-Ferrer et al., 2016). ***B***, Reconstruction of the dendritic (blue) and axonal morphology (red) of a layer 3 pyramidal HD cell recorded in a head-fixed rat. The axon is truncated for display purposes. The borders of the presubicular layers are indicated (L1–L6). Bottom, Polar plot showing the directional tuning for the representative reconstructed cell. Peak firing rate and HD index are indicated. Scale bar, 100 $\mu$m. ***C***, Schematic outline of parasagittal sections through the rat brain at three mediolateral extents of the dorsal PreS (gray): medial (top), intermediate (middle), and lateral (bottom) (see Materials and Methods for details). The locations of reconstructed tracks through the PreS (color lines) and identified cells (color dots) are represented in different colors for three representative brains (the number of recovered tracks of penetration attempts are indicated). Green arrowheads indicate the two representative tracks shown in ***D***. WM, White matter (angular bundle), Sub, subiculum, RS, retrosplenial cortex, PaS, parasubiculum. Scale bar, 500 $\mu$m. ***D***, Left, Parasagittal section stained for calbindin (green) and neurobiotin (red) showing two electrode tracks (white arrowheads) through the dorsal PreS. In the anterior penetration, spillover of Neurobiotin was performed to aid anatomical recovery of the track (see details in Materials and Methods). Right, Same section stained for NeuN (the two tracks are indicated by the arrowheads).WM, White matter (angular bundle), Sub, subiculum, RS, retrosplenial cortex. Scale bars, 200 $\mu$m.

as a pyramidal neuron (soma located at the L3/L4 border), with an ascending apical dendrite reaching the pial surface. Altogether, 11 neurons were identified, all of which were recovered in the dorsal PreS (eight cells in the superficial layers and three in the deep layers).

Third, in a total of 13 animals (including the eight mentioned above), we reconstructed all visible electrode tracks from the histological sections (Fig. 1*C*,*D*). Overall, a large fraction of electrode penetrations (120 of 149, ~80%; 13 brains) was recovered and reconstructed; of these, the large majority targeted the dorsal PreS (115 of 120; see representative reconstructions in Fig. 1*C*). Consistent with our previous study (Preston-Ferrer et al., 2016), electrode penetrations spanned the full mediolateral extent of the dorsal PreS (Fig. 1*C*) and were never observed within the retrosplenial cortex (0 of 120) and only very rarely in the subiculum (5 of 120; ~4%). We find it very unlikely that the latter minority of electrode penetration yielded HD cell recordings because, to the best of our knowledge, classical HD cells have not been reported in the subiculum and electrode penetrations could be reliably assigned to the subiculum based on the characteristic high neuronal firing rates and the abundance of bursty neurons (see details in Materials and Methods). We also note that the coordinates for recording HD cells in the retrosplenial cortex (Cho and Sharp, 2001; Jacob et al., 2017) are more medial than those used in the present study (Preston-Ferrer et al., 2016 and Material and Methods). Taken together, this evidence indicates that our HD cell recordings are very likely to stem from the dorsal PreS. We note, however, that a limitation of the present work is that the laminar location and cell-type identity of our PreS recordings could not be determined.

### Single-cell stimulation of PreS HD cells in a familiar cue-rich environment

In a first set of experiments, we tested whether evoking spike trains outside of the preferred direction in single HD cells could be sufficient for shifting and/or modifying HD tuning. Recordings were performed in a cue-rich environment in which a rich set of proximal and distal cues were available to the animal (we refer to this configuration as the Open configuration; see details in Materials and Methods). After obtaining a juxtacelluar recording from a PreS HD cell and having established its preferred direction, a spike train was evoked by brief current injections via the glass electrode (Diamantaki et al., 2016; see Materials and Methods) while the rat's head was held in place facing away from the preferred direction. A representative example is shown in Figure 2, *A–C*; here, an HD cell was recorded (Fig. 2*A*) and a spike train was evoked by juxtacellular stimulation ~150° away from the preferred direction (Fig. 2*B*). After stimulation, HD tuning remained largely unchanged compared with the baseline session (Fig. 2*C*), as indicated by the high correlation of the tuning curves (correlation coefficient = 0.95).

Altogether, we stimulated 81 HD cells (130 stimulations; see Materials and Methods and Table 1) outside of their preferred direction in a cue-rich environment. In agreement with previous juxtacellular stimulation studies (Herfst and Brecht, 2008; Houweling and Brecht, 2008), our stimulation procedures evoked spiking only in the "primary" neuron that was approached for juxtacellular stimulation; even in the rare event of a large-amplitude co-recorded "secondary" unit (peak-to-peak spike amplitude >1 mV), only the primary action potentials were modulated by the stimulation, whereas the activity of secondary units remained unaffected (seven of seven recordings; see Fig. 2-1, available at https://doi.org/10.1523/JNEUROSCI.1814-17.2018.f2-1). The advantage of our stimulation procedures (Diamantaki et al., 2016) is that they allowed us to evoke relatively long spike trains (median duration STIM trains = 6.6 s; IQR = 13.2 s; see Fig. 2*D* and Fig. 2-2, available at https://doi.org/10.1523/JNEUROSCI.1814-17.2018.f2-2), which often resembled the persistent-like activity patterns thought to play an important role in the establishment and/or maintenance of HD activity (Taube and Bassett, 2003). On average, evoked firing rates were well above the low levels of spontaneous activity at the stimulus direction (average evoked firing rate = 12.8 ± 13.1 Hz; average spontaneous firing rate = 0.7 ± 0.9 Hz; $p$ = 5.8e-23, Wilcoxon signed-rank test; see Fig. 2-2, available at https://doi.org/10.1523/ JNEUROSCI.1814-17.2018.f2-2).

To quantify possible effects of the single-cell stimulation on HD tuning, we undertook two approaches. First, we tested whether juxtacellular stimulation induced any detectable shift of preferred directions. To this end, we compared preferred directions before and after stimulations. As shown in Figure 2*E*, no significant bias toward the STIM direction was observed at the population level ($p$ = 0.67; Wilcoxon signed-rank test), with a median difference of 6.8° in preferred directions before and after stimulation ($n$ = 81). The occurrence of data points showing relatively large deviations from the identity line (8 of 81 points with Δ preferred directions >50°) was within the intrinsic variability of the HD system under our conditions; in fact, the distribution of Δ preferred directions before and after stimulation was not significantly different from the one for the two halves of the recordings in the Open configuration ($p$ = 0.73; Wilcoxon signed-rank test; Fig. 2*F*) and the fraction of neurons showing large deviations from the identity line was very similar (before vs after STIM, $n$ = 8 of 81; first vs second half, $n$ = 4 of 81). In addition, stimulations at short distances from the preferred direction were not more likely to modify HD tuning because Δ preferred directions did not significantly change as a function of stimulation distances from the preferred directions (Fig. 2*G*). This indicates that, at the population level, single-cell stimulation did not lead to detectable shifts of preferred directions.

In the second approach, we sought to estimate whether single-cell stimulation induced minor redistributions of directional firing, which was not readily apparent by simply comparing preferred directions. To this end, we used a firing-rate based quantifier. For each cell, we calculated the average firing rate within ($FR_{in}$) and outside ($FR_{out}$) a 30° interval centered on the stimulus direction (Fig. 2*H*) and then compared the ratio between the two ($Q = FR_{in}/FR_{out}$) before and after stimulation. As shown in Figure 2*I* and consistent with the representative examples (Fig. 2*A–C*,*H*), the Q ratios before and after stimulation were not significantly different (before stimulation, median = 0.12, IQR = 0.65; after stimulation, median = 0.13, IQR = 0.63; $p$ = 0.89; Wilcoxon signed-rank test). Moreover, HD tuning curves remained highly correlated (average correlation coefficient = 0.82 ± 0.32) and average HD indices virtually identical (before stimulation, 0.80 ± 0.18; after stimulation, 0.80 ± 0.21). Peak and average firing rates showed a moderate but significant increase after stimulation (peak firing rates; before stimulation, 10.3 ± 9.2 Hz; after stimulation, 12.9 ± 11.2 Hz; $p$ = 0.03; average firing rates; before stimulation, 1.6 ± 1.7 Hz; after stimulation, 2.1 ± 2.0 Hz; $p$ = 0.01; Wilcoxon signed-rank test), possibly as a result of depolarizations outlasting the (often long) evoked stimulus trains (Houweling et al., 2010).

Altogether, this indicates that, when a rich set of proximal and distal cues are available, spike trains evoked outside the preferred direction are insufficient for modifying HD tuning.

### Reduced HD tuning and average firing rates in a sensory-deprived environment

The above results suggest that, in a cue-rich environment, single-cell stimulation is insufficient for overcoming visual anchoring inputs and thus shifting the preferred direction of HD neurons. We hypothesized that single-cell stimulation could be more efficient in a sensory-deprived environment, where anchoring visual inputs are drastically reduced. To this end, we reduced the number of available landmarks to a single proximal visual cue. We found that, in our head-fixed preparation, this manipulation led to an erratic behavior of HD cells (Knierim et al., 1998), characterized by a reduction in average firing rates (see also Pérez-Escobar et al., 2016) accompanied by a rapid destabilization of HD tuning. This is shown in the representative recording in Figure 3, *A–C*. Here, a HD cell was first recorded in the Open configuration with spiking activity occurring within a narrow HD angle (HD index = 0.92; Fig. 3*A*). Then, a cylinder was lowered around the animal (referred to as the Closed configuration), which prevented access to distal cues and only a single proximal visual cue was available (LED1; Fig. 3*B*). When recorded in the Closed configuration, the HD cell rapidly lost its directional tuning (HD index = 0.20; $p$ = 0.11, Rayleigh test; Fig. 3*B*,*D*), as indicated by the larger spread of spikes as a function of HD (Fig. 3*D*). The average firing rate also decreased from 3.3 Hz in the Open to 2.3 Hz in the Closed configuration. Once tested again in the Open configuration, both the average firing rate and head directionality recovered toward baseline levels (Fig. 3*C*).

Altogether we sequentially monitored the activity of 69 HD cells in the Open and then in the Closed configuration (Fig. 3*E*). In the latter configuration, a clear decline of both average firing

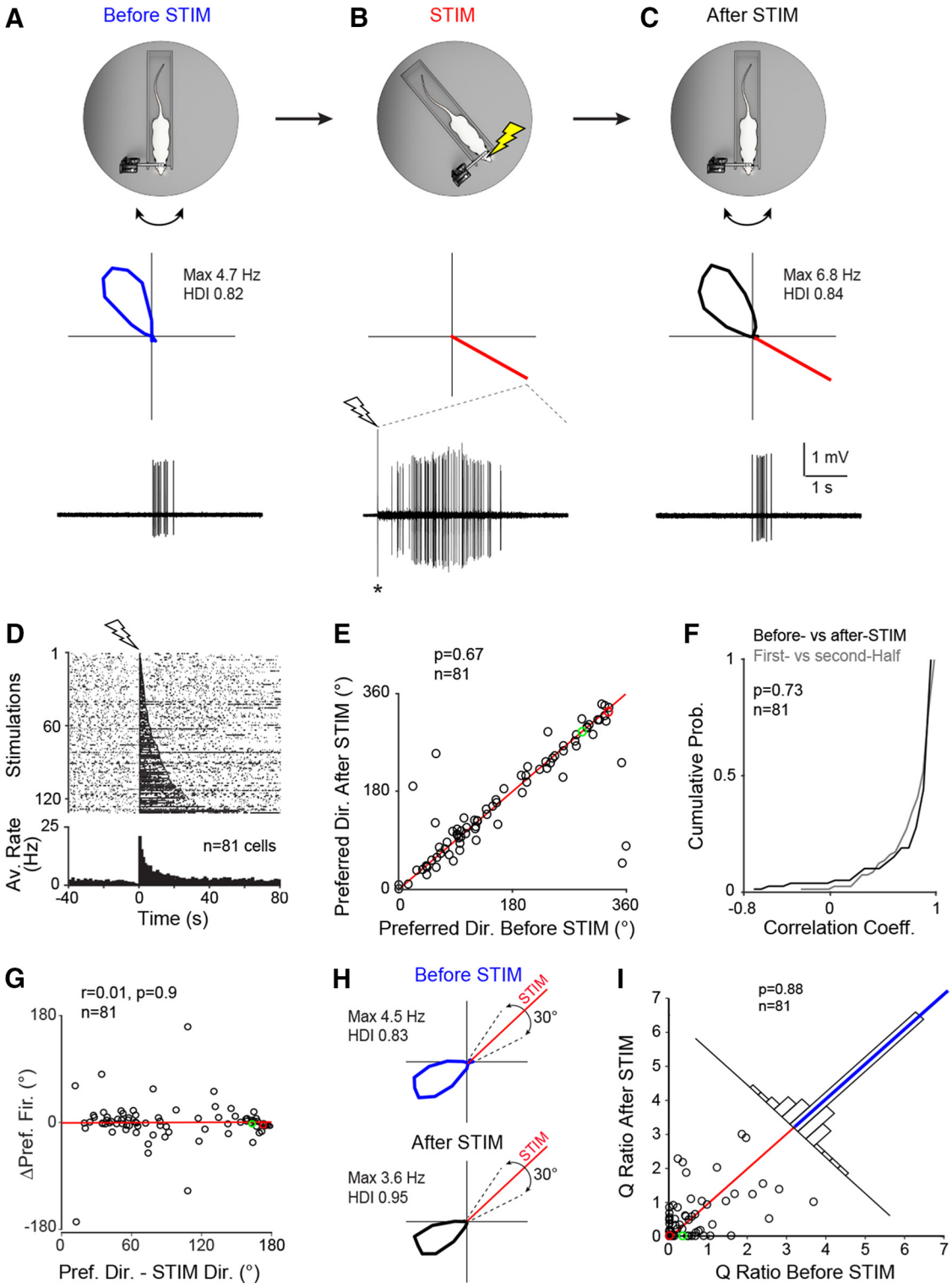


**Figure 2.** Single-cell stimulation in a cue-rich familiar environment. ***A***, Top, Schematic representation of the Open recording configuration consisting of a head-fixed rat on a rotating platform in the presence of a rich set of proximal and distal cues (see also Preston-Ferrer et al., 2016). Middle, Polar plot showing firing rate as a function of HD for a representative PreS HD neuron recorded during passive rotation. Peak firing rate and HD index are indicated. Bottom, High-pass-filtered spike trace for the HD cell recording shown above. ***B***, Same as ***A*** but for juxtacellular stimulation (STIM) at ~150° away from the preferred direction. The polar plot (middle) indicates the stimulus direction (red line). Bottom, High-pass-filtered voltage trace showing a spike train evoked by a brief juxtacellular current injection (see Materials and Methods). The onset of current injection is indicated by the lightning bolt symbol. The asterisk indicates stimulus artifact, truncated for display purposes. ***C***, Same as in ***A*** but after the juxtacellular stimulation shown in ***B***. Note that HD tuning remained largely unchanged compared with before stimulation (***A***). ***D***, Raster plot (top) and average firing rate histogram (bottom) for all spike trains evoked in HD neurons under passive rotation ($n = 130$ stimulations in 81 neurons). Recordings are aligned by the first spike of the evoked stimulus train (lightning bolt symbol). For display purposes, all stimulations are shown in the raster plot; however, multiple stimulations within individual neurons were averaged before being entered into the firing rate histogram so that each cell contributed one data point. ***E***, Scatterplot showing preferred directions computed before and after the stimulation. Red line indicates the identity line. The red and green circles correspond to the representative examples shown in ***A***–***C*** and ***H***, respectively. The number of cells and the *p*-value (Wilcoxon signed-rank test) are indicated. ***F***, Cumulative probability plot showing the correlation coefficients for HD tuning curves computed before and after stimulation (black) and for the two halves of the (*Figure legend continues.*)

**Table 1. STIM-Open, STIM-Closed, and No-STIM datasets**

| Dataset | No. of rats[a] | No. of cells | No. of STIM | Recorded duration before STIM (s) | STIM duration (s)[b] | Recorded duration after STIM (s) | HD index (in Open)[c] | Average firing rate in Open (Hz)[c] | Peak firing rate in Open (Hz)[c] |
|---|---|---|---|---|---|---|---|---|---|
| STIM-Open | 18 | 81 | 130 | 86.2 (51.4) | 10.0 (14.1) | 63.1 (32.8) | 0.87 (0.25) | 1.3 (1.6) | 4.6 (5.9) |
| STIM-Closed | 7 | 25 | 42 | 64.2 (23.0) | 8.2 (11.8) | 60.7 (19.0) | 0.85 (0.31) | 1.7 (1.8) | 6.4 (7.5) |
| No-STIM | 6 | 25 | 35 | 50.2 (16.2) | 20.6 (6.1) | 55.6 (19.1) | 0.92 (0.25) | 1.4 (0.9) | 5.2 (9.8) |

[a]Note that the total number of rats used in the STIM-Open, STIM-Closed, and No-STIM datasets is 26 (see Materials and Methods) because individual rats typically contributed to more than one dataset. For detailed information, see Table 1-1 (available at https://doi.org/10.1523/JNEUROSCI.1814-17.2018.t1-1).

[b]Time that animals spent facing the stimulus direction during juxtacellular stimulation (calculated as the time between offset and onset of passive rotation; see Materials and Methods).

[c]Basic properties of the HD cells (HD index, average firing rates, and peak firing rates), assessed in the Open configuration, were not significantly different between the three datasets (STIM-Open, STIM-Closed, and No-STIM; all $p$ values larger than 0.165; Wilcoxon rank-sum test with Bonferroni correction).

Data are shown as median and IQR (in parentheses).

rates (Open, 2.35 ± 2.20 Hz; Closed, 1.42 ± 1.67 Hz; $p = 1.3e-7$; Wilcoxon signed-rank test) and head directionality (Open, 0.82 ± 0.17; Closed, 0.50 ± 0.29; $p = 7.0e-7$; Wilcoxon signed-rank test; Fig. 3*F*,*G*) was observed at the population level, with a consistent fraction of recordings (18 of 69; ~26%) falling below our HD criteria (see representative examples in Fig. 3*F*). A fraction of HD cells remained stable in the Closed configuration, as indicated by the high correlation between the corresponding tuning curves (14 of 69 cells with correlation coefficients > 0.8; ~20%), suggesting that these neurons might correspond to a specific subpopulation of PreS HD cells. However, simultaneous recordings of multiple HD neurons will be required for testing this hypothesis. Average firing rates of putative fast-spiking interneurons ($n = 11$; see Materials and Methods) were also reduced in the Closed configuration (Open, 36.6 ± 15.9 Hz; Closed, 27.1 ± 12.5 Hz; $p = 0.001$; Wilcoxon signed-rank test). This observation is compatible with the reduction of a common visual input to the PreS HD network affecting both principal neurons as well as feedforward inhibitory cells; however, a reduced local excitatory drive to feedback interneurons could also account for the observed firing rate reduction.

After sequential recording in the Open–Closed configuration, a subset of cells ($n = 23$) were tested again in the Open configuration (Open1–Closed–Open2; as shown in Fig. 3*A*–*D*). HD tuning for the majority of the tested neurons recovered to baseline levels, as indicated by the high correlation coefficients between tuning curves computed in the Open1 and Open2 configurations (Fig. 3*H*). In the Open2, average HD indices (Fig. 3*I*) and peak firing rates (Open1, 7.35 ± 7.23; Open2, 7.13 ± 7.34; $p = 0.88$; Wilcoxon signed-rank test) largely recovered to the baseline values assessed in Open1, indicating that the loss of directionality was rather selective for the Closed configuration. However, not all neurons recovered to baseline tuning (Fig. 3*I*), an observation in agreement with earlier work reporting an incomplete recovery of directionality after a dark session in passively rotated rats (Knierim et al., 1998).

Because both average firing rates and head directionality were strongly reduced in the Closed configuration, we sought to test whether the observed loss of directional tuning was a simple consequence of the firing rate reduction. To this end, we downsampled the spiking during each recording trial in the Open configuration to match the spike rate observed during the following trial in the Closed configuration. After downsampling, HD indices remained significantly higher in the Open compared with the Closed configuration (downsampled, 0.83 ± 0.17; Closed, 0.50 ± 0.29; $p = 1.9e-10$; Wilcoxon signed-rank test), indicating that the loss of directionality in the Closed configuration was not a mere consequence of the firing rate reduction.

In a subset of neurons ($n = 11$), firing rates were also monitored in the absence of visual cues (Dark configuration). Consistent with recent work (Pérez-Escobar et al., 2016), average firing rates of HD cells were significantly lower in the Dark compared to the Closed configuration (Closed, 6.6 ± 3.2; Dark, 3.9 ± 3.8 Hz, $p = 9.8e-4$; Wilcoxon signed-rank), indicating that visual inputs reaching the PreS might be necessary for sustaining PreS neuronal firing rates to physiological levels. To explore this issue further, we performed multiunit extracellular recordings in anesthetized rats while light-flash stimuli (2 s long) were presented to the contralateral eye (Fig. 4*A*). As shown in the representative recording, which was localized to the PreS via anatomical verification of an electrolytic lesion (Fig. 4*B*), the light-flash stimulus induced a sustained increase in firing rates (Fig. 4*C*). This effect was significant at the population level by including all recording sites that could be assigned to the PreS ($n = 14$, Fig. 4*D*; average response latencies, 113 ± 39 ms; see details in Materials and Methods). This electrophysiological evidence thus supports the known anatomical connectivity between PreS and upstream visual areas (Vogt and Miller, 1983; Caballero-Bleda and Witter, 1993, 1994; Ding, 2013) and indicates that PreS neuronal firing rates are modulated by visual inputs.

## HD cell realignment after cue rotations

Previous work from freely moving rodents has demonstrated that salient visual cues can exert control over HD signals. Realignment of HD signals can be rapidly and consistently induced by the rotation of polarizing visual landmarks such as cue cards or light cues (Taube et al., 1990a; Goodridge and Taube, 1995; Taube and Burton, 1995; Taube, 1995a,b; Goodridge et al., 1998; Zugaro et al., 2000; Knight et al., 2014). In a subset of experiments, we tested whether, in our head-fixed preparation, cue rotations could induce a corresponding shift in the preferred directions of HD neurons. To this end, after obtaining a recording from a HD cell

←

(*Figure legend continued.*) recordings before stimulation (gray). The number of cells and the $p$-value are indicated. ***G***, Scatter plot showing Δ preferred directions (i.e., preferred direction after stimulation-preferred direction before stimulation) as a function of the stimulus distance from the preferred direction (i.e., preferred direction-STIM direction). The red and green circles correspond to the representative examples shown in ***A***–***C*** and ***H***, respectively. The linear regression line (red), the correlation coefficient ($r$), the number of cells, and the $p$-value are indicated. ***H***, Polar plots showing the activity of another HD cell before and after the stimulation (rotated by 45° for display purposes). Dotted lines indicate the 30° interval centered on the stimulus direction (red line) used for computing the Q ratios (see ***I*** and text for more details). Peak firing rates and HD indices are indicated. ***I***, Scatterplot showing the Q ratios (i.e., the ratios between the average firing rate within and outside a 30° interval centered on the stimulus direction) computed for all cells before and after the stimulation. The red and green circles correspond to the representative examples shown in ***A***–***C*** and ***H***, respectively. Red line indicates the identity line and the blue line on the top histogram represents the median. The number of cells and the $p$-value (Wilcoxon signed-rank test) are indicated. More details about the stimulation procedures can be found in Figures 2-1 (available at https://doi.org/10.1523/JNEUROSCI.1814-17.2018.f2-1) and 2-2 (available at https://doi.org/10.1523/JNEUROSCI.1814-17.2018.f2-2).

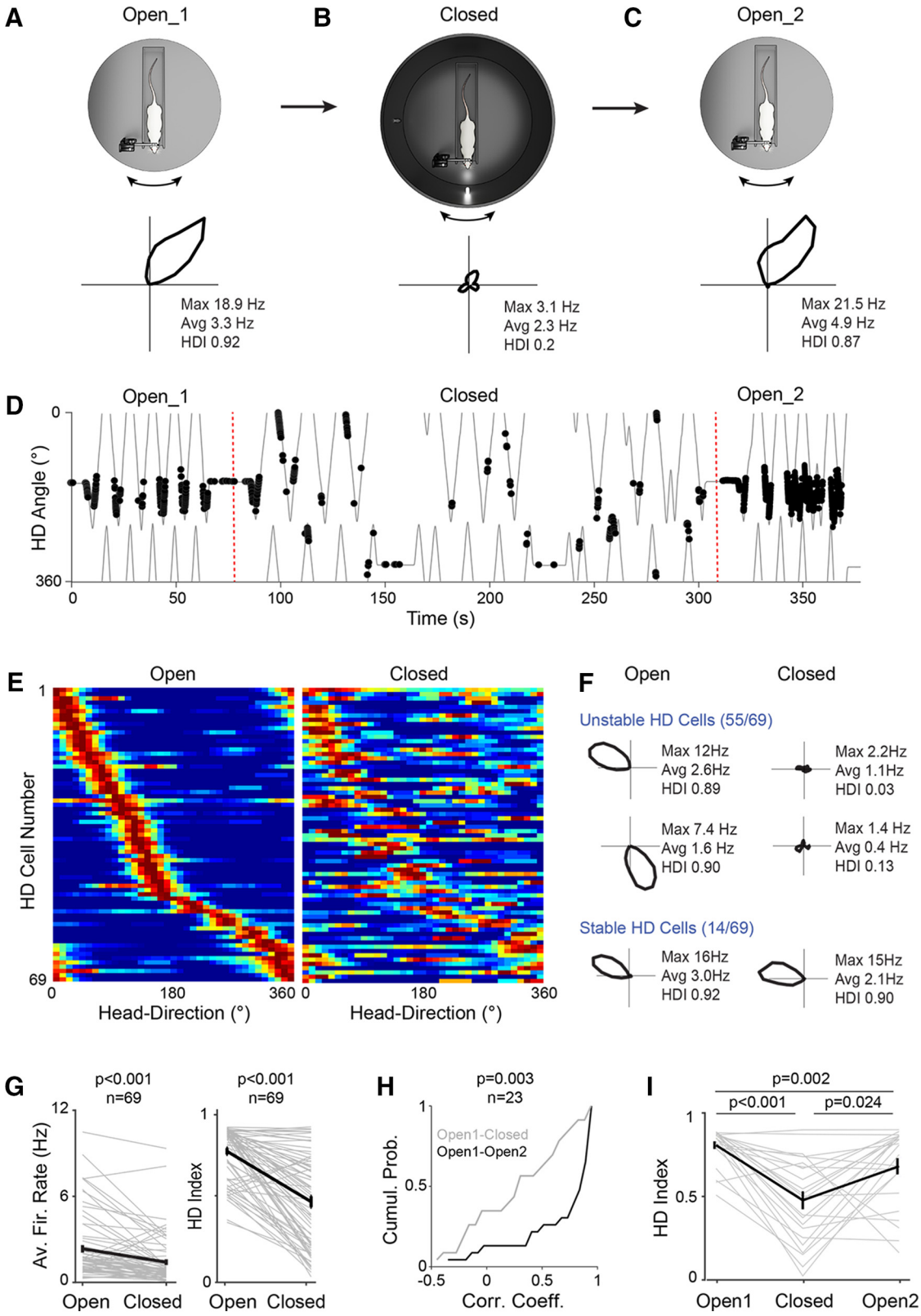


**Figure 3.** Unstable HD activity in the presence of a single proximal visual cue. ***A–C***, Top, Schematic representation of the recording protocol in which the activity of the neurons ($n = 69$) was sequentially monitored in the Open (***A***, Open_1) and Closed (***B***) configuration. For a subset of neurons ($n = 23$), the activity was monitored in the Open configuration again (***C***, Open_2). Note the presence of a cylinder surrounding the animal and a single proximal visual cue (LED) in the Closed configuration. Bottom, Polar plots showing firing rate as a function of HD for a representative HD cell recorded sequentially in the Open_1, Closed, and Open_2 configurations. Peak and average firing rates and HD indices are indicated. ***D***, Spike trajectory plot showing the angular HD as a function of time for the same cell shown in ***A–C***. Spikes (black dots) are indicated. The dotted red line indicates the transition across the different configurations. Note the sharp HD tuning of the cell in both Open Configurations (Open_1 and Open_2) compared with the Closed configuration (Closed). ***E***, Color-coded distribution of preferred direction for all HD cells ($n = 69$) recorded sequentially in the Open (left) and Closed (right) configurations. Each row represents the firing rate of a single neuron (normalized relative to its peak firing rate; red) ordered by the location of their peak firing rates relative to the rat's HD in the Open Configuration. ***F***, Polar plots showing the activity of representative "stable" and "unstable" HD cells (*Figure legend continues.*)

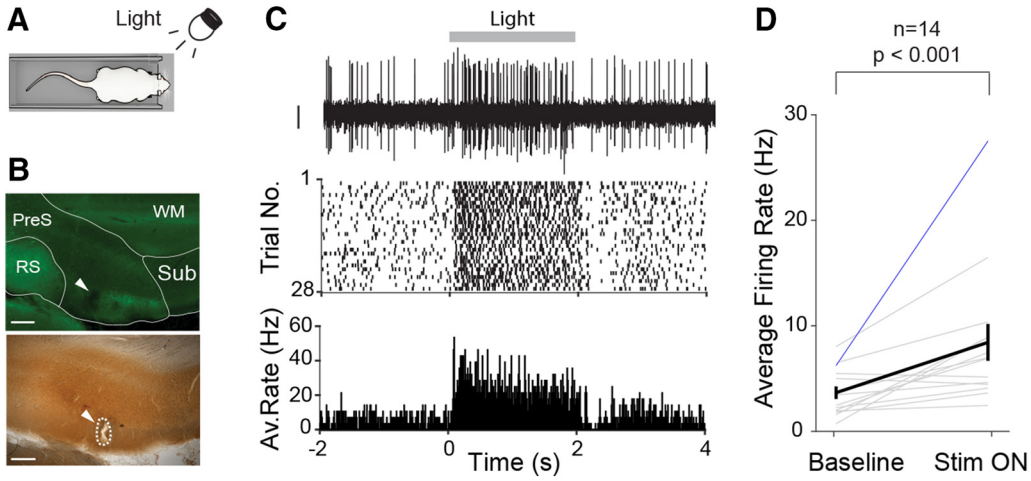


**Figure 4.** Extracellular recordings of visual responses in the PreS of anesthetized rats. ***A***, Schematic representation of the experimental configuration. Multiunit extracellular recordings were performed in anesthetized rats while light-flash stimuli (2 s) were presented to the contralateral eye (see Materials and Methods for details). ***B***, Parasagittal section through the dorsal PreS stained for calbindin (green; top) and cytochrome-oxidase activity (bottom). The electrolytic lesion site (dotted line), corresponding to the location of the extracellular recording shown in ***C***, is indicated by the arrowhead. WM, White matter (angular bundle); Sub, subiculum; RS, retrosplenial cortex. Scale bars, 200 $\mu$m. ***C***, Top, Representative high-pass filtered voltage trace showing the increase in multiunit activity evoked by the visual stimulus. The duration of the stimulation presentation (light) is outlined by the gray bar (2 s). The raster plot (middle) and the peristimulus time histogram (bottom) for all stimulation trials ($n = 28$) are shown. ***D***, Average firing rates computed for 0.5 s before (baseline) and 0.5 after (Stim ON) the onset of the visual stimulus ($n = 14$ neurons). Black line indicates the average, blue line the recording shown in ***C***. Error bars indicate SEM. *p*-value is indicated (Wilcoxon signed-rank test).

in the Closed configuration (LED1; as in Fig. 5*A*) and after a brief dark phase, the visual cue was rotated 90° away from its original position (Fig. 5*A*; LED1→LED2). As can be seen in Figure 5*B* and consistent with previous work from freely moving animals (Knierim et al., 1998; Zugaro et al., 2000, 2003), already from the first pass the neuron's preferred direction was realigned to the new cue location. After another brief dark phase, the visual cue was then shifted back to its original position (Fig. 5*A*; LED2→LED1), which was again followed by a rapid and coherent realignment of the neuron's preferred direction (Fig. 5*B*,*C*).

Altogether, we recorded 11 HD cells following the experimental protocol shown in Figure 5*A* (see Materials and Methods). Despite the reduction in HD tuning observed in the Closed configuration (Fig. 3), the preferred direction of all neurons tested was reliably controlled by the single light cue. The average shift in the preferred directions was slightly <90° (83.6° ± 14.3°; see Fig. 5*D*), with under-rotations being slightly more common than over-rotations, remarkably consistent with previous work from freely moving rodents (Taube et al., 1990a; Goodridge and Taube, 1995; Knierim et al., 1995; Taube and Burton, 1995; Taube, 1995a; Dudchenko et al., 1997; Goodridge et al., 1998; Knight et al., 2014).

These data indicate that, despite the reduced HD selectivity in the Closed configuration (Fig. 3), a single proximal visual cue is able to gain control over the residual HD signals.

←

(*Figure legend continued.*) sequentially recorded in the Open and the Closed configuration. Peak and average firing rates and HD indices are indicated. ***G***, Average firing rates and HD indices computed in the Open and Closed configuration ($n = 69$ neurons, gray lines). Black lines indicate the averages. Error bars indicate SEM. *p*-values are indicated (Wilcoxon signed-rank test). ***H***, Cumulative probability plot showing the correlation coefficients of HD tuning curves for the Open_1 versus Closed configuration (gray) and for the Open_1 versus Open_2 configuration (black). The number of cells and the *p*-value (Wilcoxon signed-rank test) are indicated. ***I***, HD indices computed in the Open_1, Closed, and Open_2 configurations ($n = 23$ neurons, gray lines). Black line indicates the average. Error bars indicate SEM. *p*-values are indicated (Wilcoxon signed-rank test; Bonferroni correction for multiple comparisons).

**Single-cell stimulation under "instability" of the HD system**

The above results indicate that, in the Closed configuration, in which anchoring visual inputs are reduced, the HD system is largely destabilized (Fig. 3). In a subset of experiments, we tested whether, under these conditions, inducing strong postsynaptic spiking via juxtacellular stimulation would be sufficient for biasing neuronal output. A representative example is shown in Figure 6, *A–D*. Here, a HD cell was recorded in the Open configuration (HD index = 0.95; Fig. 6*A*), which then showed weaker directional tuning in the Closed configuration (HD index = 0.54; Fig. 6*B*). A spike train was evoked by juxtacellular stimulation away from the neuron's preferred direction (Fig. 6*C*); as can be seen in Figure 6*D*, after stimulation, the neuron showed increased activity at the stimulus direction.

Altogether, we recorded and stimulated 25 PreS neurons (42 stimulations; Table 1) in the Closed configuration following the experimental protocol shown in Figure 6, *A–D*. Before this protocol, the large majority of the neurons (23 of 25) were also recorded in the Open configuration and were classified as HD cells (Table 1); consistent with the previous results (Fig. 3), both HD indices and average firing rates were markedly reduced in the Closed configuration (HD indices, Open = 0.80 ± 0.16; Closed = 0.36 ± 0.24; $p = 2.1e\text{-}5$; average firing rates, Open = 2.1 ± 2.0 Hz; Closed = 1.2 ± 1.2 Hz; $p = 0.005$; Wilcoxon signed-rank test). Juxtacellular stimulation procedures, as well as evoked and spontaneous firing rates at the stimulus direction (average evoked firing rate = 12.9 ± 10.2 Hz; average spontaneous firing rate = 1.0 ± 1.8 Hz; $p = 1.6e\text{-}8$, Wilcoxon signed-rank test; Fig. 6*E*), were not significantly different from the ones in the Open configuration (Fig. 2-2, available at https://doi.org/10.1523/JNEUROSCI.1814-17.2018.f2-2); however, unlike for the latter experiments, Q ratios were significantly increased after stimulation (before stimulation, median = 0.20, IQR = 0.59; after stimulation, median = 0.63, IQR = 0.96; $p = 0.003$; Wilcoxon signed-rank test; Fig. 6*F*,*G*), indicating a redistribution of spiking activity around the stimulus direction. This effect did not critically depend upon the choice of the angu-

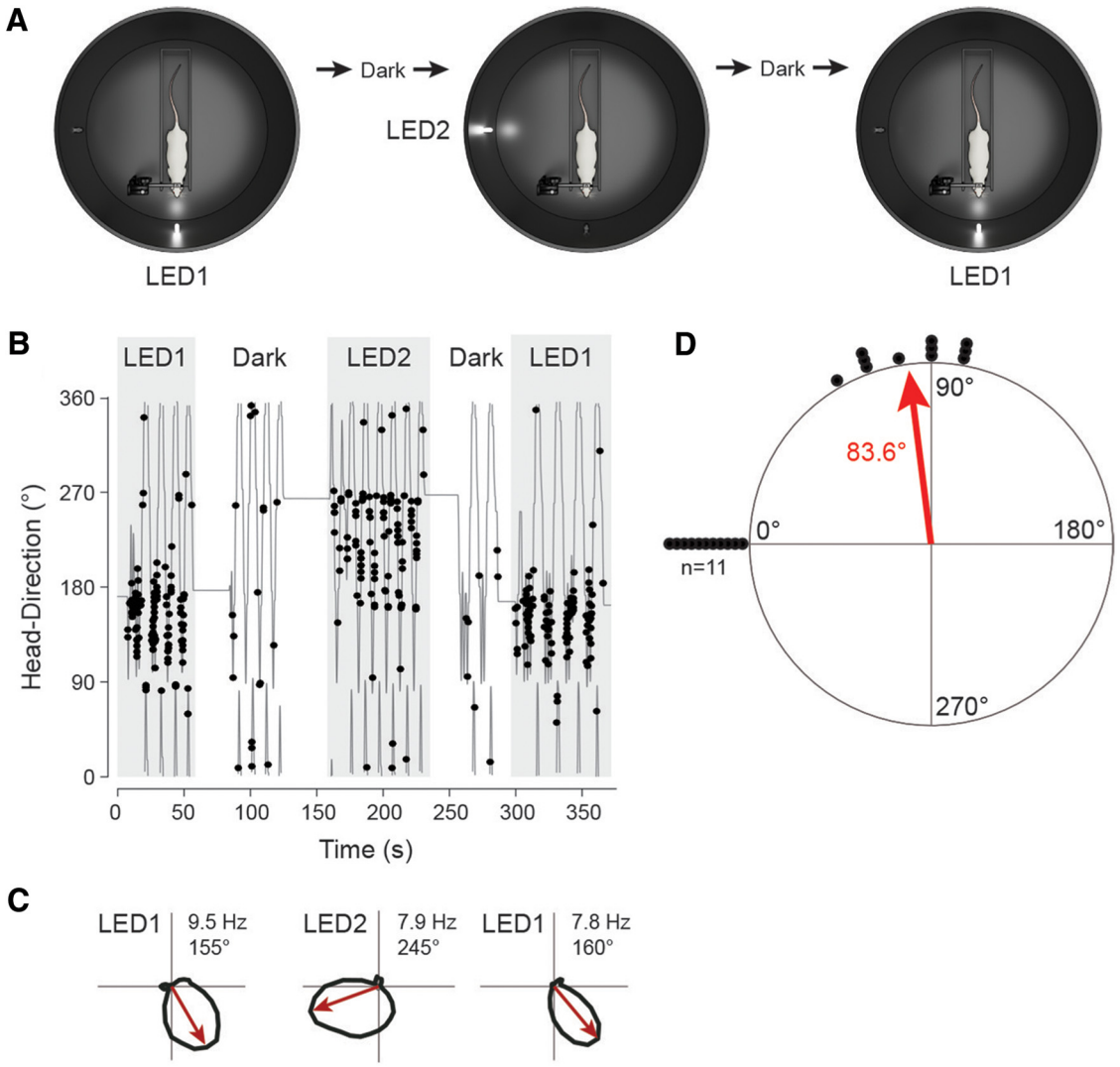


**Figure 5.** HD cell realignment after cue rotations. ***A***, Schematic drawing showing the recording protocol for 90° cue rotations (LED1⟶LED2 and LED2⟶LED1). Cue rotations were interleaved with brief dark phases (see Materials and Methods for details). ***B***, Angular HD as a function of time for a representative HD cell recorded following the protocol shown in ***A***. Spikes (black dots) are indicated. Note the consistent shift of the neuron's preferred direction upon cue rotations (LED1⟶LED2 and LED2⟶LED1). ***C***, Polar plots showing firing rates as a function of HD computed for LED1 (left), LED2 (middle), and the return to LED1 (right) for the same cell shown in ***B***. Preferred directions (red arrows) and peak firing rates are indicated. ***D***, Scatter diagrams showing the amount of angular shift of preferred directions between LED1 and LED2 configurations. Each dot represents a single cell ($n = 11$). The preferred directions shown by all cells in the LED1 configuration are aligned at 0°; therefore, those shown during the LED2 configuration are represented clockwise (because LED2 was placed 90° clockwise with reference to LED1). The average angle is indicated by the red arrow.

lar range used for computing the Q ratios (30° centered on the stimulus direction; as schematically represented in Fig. 6*F*) because similar results were obtained with 60° and 90° angles (data not shown). The single-cell stimulation effect was small at the population level (see mean shift from the identity line in Fig. 6*G*); however, a peak around the stimulus direction could still be detected from the population data by calculating the difference between the average tuning curves before and after stimulation (Fig. 6*H*). We acknowledge that the instability of the HD signals in the Closed configuration represents a limitation for assessing stimulation effects. To circumvent this limitation, we restricted the analysis to the small subset of neurons that retained significant HD tuning in the Closed configuration ($n = 8$). We found that Q ratios were significantly increased after stimulation ($p = 0.039$; Wilcoxon signed-rank test) and the distances between stimulus and preferred directions became significantly smaller after stimulation (before stimulation, 147 ± 21°; after stimulation, 102 ± 58°; $p = 0.039$; Wilcoxon signed-rank test), indicative of a shift toward the stimulus direction. Although consistent with the conclusions from the STIM-Closed dataset (Fig. 6), we acknowledge that this evidence rests on a small number of observations.

To verify that the small stimulation effect (Fig. 6*G*,*H*) reflected a true redistribution of firing around the stimulus direction, we performed the following controls.

First, we compared HD indices and spike shapes before and after stimulation. Because our metric for quantifying stimulation effect (Q ratio) is sensitive to the circular distribution of spike rates, aspecific effects (e.g., broadening of tuning curves and/or cellular damage after stimulation) could possibly determine an increase in Q ratios. However, HD indices before and after stimulation were not significantly different (before stimulation, 0.37 ± 0.24; after stimulation, 0.40 ± 0.22; $p = 0.69$; Wilcoxon signed-rank test). Similarly, spike shapes, the features of which can serve as a clear indicator of cellular damage (Herfst et al., 2012), remained very similar (e.g., spike half-widths; before stimulation, 0.30 ± 0.03 ms; after stimulation, 0.32 ± 0.05 ms; $p = 0.06$;

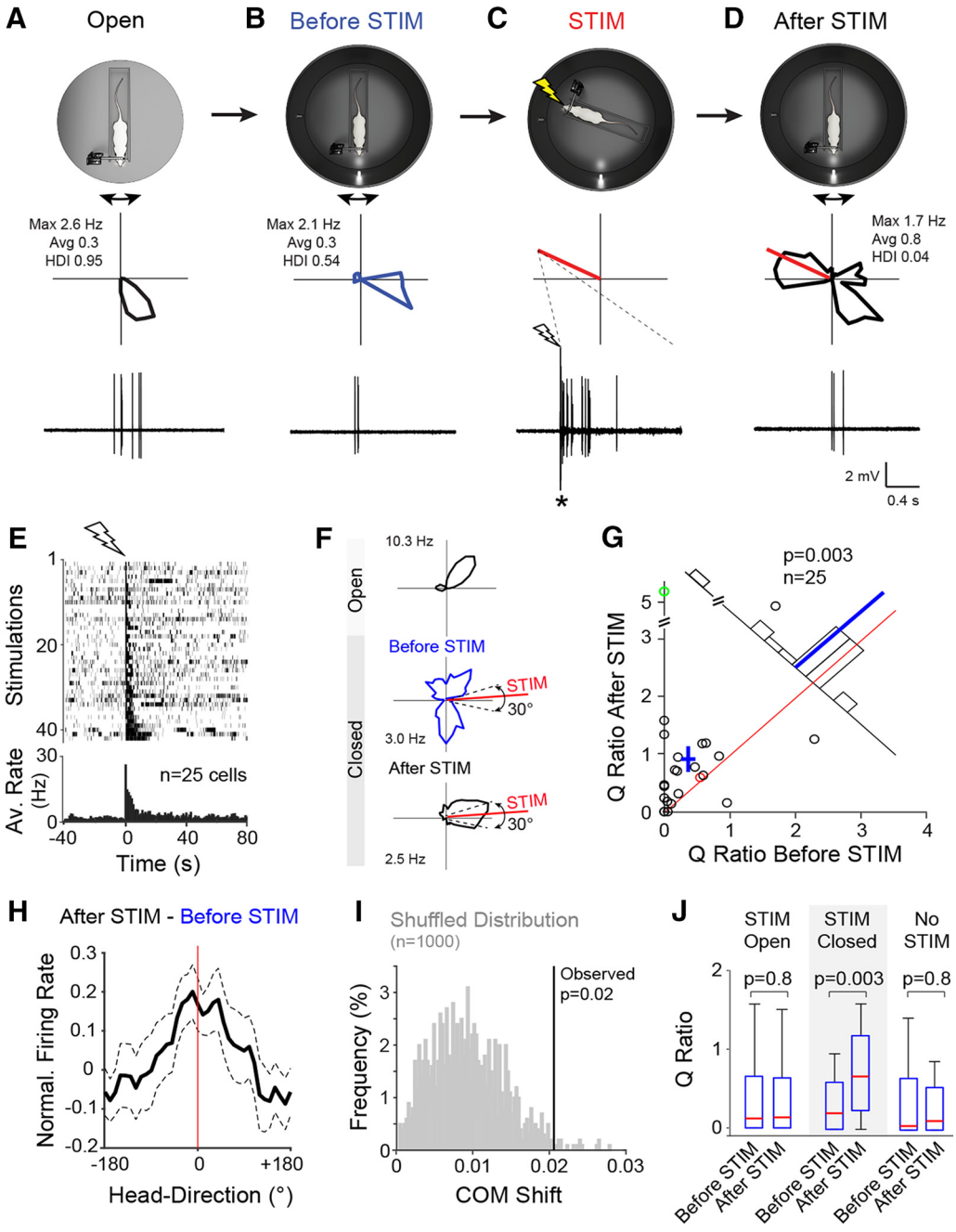


**Figure 6.** Single-cell stimulation under "instability" of the HD system. ***A***, Top, Schematic representation of the Open recording configuration consisting of a head-fixed rat on a rotating platform in the presence of a rich set of proximal and distal cues. Middle, Polar plot showing firing rate as a function of HD for a representative PreS HD neuron recorded during passive rotation. Peak and average firing rates and HD indices are indicated. Bottom, High-pass-filtered spike trace for the HD cell recording shown above (scale bars as in ***D***). ***B***, Same as ***A*** but for the Closed recording configuration. ***C***, Same as ***A*** but for juxtacellular stimulation (STIM). The polar plot (middle) indicates the stimulus direction (red line). Bottom, High-pass filtered voltage trace showing a spike train evoked by a brief juxtacellular current injection (see Materials and Methods). The onset of current injection is indicated by the lightning bolt symbol. The asterisk indicates stimulus artifacts truncated for display purposes. Scale bars are as in ***D***. ***D***, Same as in ***B*** but after the juxtacellular stimulation shown in ***C***. Note the redistribution of firing around the stimulus direction (red line). ***E***, Raster plot (top) and average firing rate histogram (bottom) for all spike trains evoked in PreS neurons under passive rotation ($n = 42$ stimulations in 25 neurons). Recordings are aligned by the first spike of the evoked stimulus train (lightning bolt symbol). For display purposes, all stimulations are shown in the raster plot; however, multiple stimulations within individual neurons were averaged before being entered into the firing rate histogram, so that each cell contributed one data point. ***F***, Polar plots showing the activity of another HD cell in the Open and before and after the stimulation (HD indices: Open, 0.65; before STIM, 0.07; after STIM, 0.61; average firing rates: Open, 2.9 Hz; before STIM, 1.4 Hz; after STIM, 1.2 Hz; peak firing rates are indicated). Dotted lines indicate the 30° interval centered on the stimulus direction (red line) used for computing the Q ratios (see ***G*** and text for more details). ***G***, Scatterplot showing the Q ratios (i.e., the ratios between the average firing rate within and outside a 30° interval centered on the stimulus direction) computed for all cells before and after the stimulation. The red and green circles correspond to the representative examples shown in ***A***–***D*** and (***F***), respectively. Red line indicates the identity line, blue cross the mean ± SEM, and blue line the mean. The number of cells and the *p*-value (Wilcoxon signed-rank test) are indicated. ***H***, Graph showing the subtraction of the average normalized tuning curves computed before and after stimulation (After STIM-Before STIM) aligned at the stimulus direction (0°). Note that a peak becomes apparent around the stimulus direction (red line). Dashed lines show SEM. ***I***, Shuffled distribution of COM shifts (gray) computed by randomly shuffling individual recording epochs before and after stimulation (see details in Materials and Methods). The observed COM shift for the STIM-Closed dataset (vertical line) and the corresponding *p*-value are indicated. ***J***, Box pots showing the Q ratios computed before and after stimulation for each dataset (STIM-Open, STIM-Closed, and No-STIM). Whiskers represent 1.5 IQR. Outliers are not shown for display purposes. *p*-values are indicated (Wilcoxon signed-rank test). More details about the STIM-Closed and No-STIM datasets can be found in Table 1.

spike peak-to-trough; before stimulation, 0.55 ± 0.10 ms; after stimulation, 0.60 ± 0.12 ms; $p = 0.09$; Wilcoxon signed-rank test), thus ruling out a systematic broadening of tuning curves and/or cellular damage as a result of single-cell stimulation.

Second, because average firing rates were significantly increased after stimulation in the Closed dataset (before stimulation, 1.3 ± 1.3 Hz; after stimulation, 2.1 ± 1.7 Hz; $p = 0.002$; Wilcoxon signed-rank test), we verified that the observed biasing effect of single-cell stimulation was not a simple consequence of the increased firing. Indeed, we found that downsampling spike rates in each after stimulation trial to match the spike rates observed during the respective before stimulation trial led to qualitatively similar results (Q ratios; before stimulation, median = 0.20, IQR = 0.59; after stimulation, median = 0.76, IQR = 0.87; $p = 0.001$; Wilcoxon signed-rank test).

Third, to assess the significance of our single-cell stimulation effect, we performed a label-shuffling test. For each shuffle, all recording epochs before and after individual stimulations were randomly assigned the labels "before stimulation" or "after stimulation" (see details in Materials and Methods) and a modulation index was computed (Q ratio after STIM − Q ratio before STIM)/(Q ratio after STIM + Q ratio before STIM). The observed average modulation index (= 0.35) was larger than the 95$^{th}$ percentile of the null distribution (constructed from 1000 shuffles; $p = 0.01$), indicating that the small stimulation effect is unlikely to arise from a random redistribution of spiking activity (a spike-time shuffling test led to qualitatively similar results; $p = 0.040$; see Material and Methods). Moreover, single-cell stimulation resulted in a small but significant COM shift of the average HD tuning curves toward the stimulus direction ($p = 0.02$, $n = 25$; Fig. 6*I*; average shift direction = 3.5°, where 0° indicates the stimulus direction).

Fourth, to test whether the stimulation effect was dependent upon single-cell stimulation, we performed a subset of control experiments in which the rat's head was kept stationary away from the neurons' preferred direction, but no stimulation was performed (No-STIM dataset; $n = 25$). Before recording in the Closed configuration, all neurons were also recorded in the Open configuration and were classified as HD cells. The basic properties of these HD neurons were very similar to the ones in the STIM-Closed dataset (e.g., average HD index, peak, and average firing rate; Table 1), thus ruling out a systematic bias in sampling HD neurons across the two datasets. In the Closed configuration, average firing rates during No-STIM epochs remained at baseline levels (average firing rate during No-STIM = 0.75 ± 1.0 Hz; average spontaneous firing rate at the No-STIM direction = 0.74 ± 1.9 Hz; $p = 0.08$; Wilcoxon signed-rank test; Fig. 2-2, available at https://doi.org/10.1523/JNEUROSCI.1814-17.2018.f2-2) and, indeed, in the absence of stimulation, no redistribution of firing was observed around the No-STIM direction, as indicated by the fact that Q ratios computed before and after no stimulation were not significantly different (before stimulation, median = 0.02, IQR = 0.66; after stimulation, median = 0.12, IQR = 0.54; $p = 0.8$; Wilcoxon signed-rank test; Fig. 6*J*). The average modulation index (= 0.072) was also not significantly larger than the shuffled data ($p = 0.31$). These data indicate that, in a sensory-deprived environment, single-cell stimulation can induce a small activity bias in single PreS neurons toward the stimulus direction.

## Discussion

In recent years, single-cell stimulation has proven to be a viable approach for probing the plasticity rules of individual neurons in the intact brain during behavior. To date, the most striking examples have been obtained in the rodent hippocampus, where intracellular manipulations of activity (Bittner et al., 2015, 2017) or excitability (Lee et al., 2012; Christenson et al., 2016) have resulted in the rapid appearance of place fields. Using similar juxtacellular stimulation procedures as in the present study, we have also found that the output of a consistent fraction of neurons in the dentate gyrus (Diamantaki et al., 2016) and in the CA1/CA3 regions (unpublished observations) can be rapidly biased by the evoked activity. Consistent with this evidence, we sought to test whether juxtacellular stimulation of individual PreS neurons was equally able to induce plastic changes in HD tuning. We found, however, that in a cue-rich environment, juxtacellular stimulation did not result in any detectable modification of HD activity (Fig. 2). Even seconds-long evoked spike trains (Fig. 2*D* and Fig. 2-2, available at https://doi.org/10.1523/JNEUROSCI.1814-17.2018.f2-2) failed to induce a significant shift in preferred directions. We think this observation is consistent with the postulated organization of HD neurons as part of an attractor network, the recurrent architecture of which ensures stability of the activity hill against external "noise." Resisting disturbances from single neurons might be an important feature of the HD system, which guarantees its functioning as a coherent unit. Our evidence thus supports fundamentally distinct architectures of hippocampal place and PreS HD networks: whereas place cells are highly plastic (thus consistent with their postulated role in the encoding of episodic information), HD neurons are highly insensitive to activity manipulations (thus fulfilling the stability requirement for an internal "sense of direction").

However, we found that, under specific conditions (i.e., reduced visual landmarks in our head-fixed preparation; Fig. 6), stimulus-induced postsynaptic spiking was able to bias HD activity in individual PreS neurons. This observation is consistent with recent work (Kim et al., 2017) showing that, in the absence of visual cues, an ectopic and transient activity hill on the *Drosophila* ellipsoid body ring attractor (Seelig and Jayaraman, 2015; Wolff et al., 2015) could be induced by optogenetic stimulation. Although, in the latter study, it was possible to target and stimulate a population of neurons with similar tuning properties given their topographical arrangement on an anatomical ring structure (Seelig and Jayaraman, 2015; Wolff et al., 2015), in our study, only individual HD cells were stimulated. Therefore, we find it unlikely that our biasing effect on single-cell activity reflects a global reorientation of the HD attractor because attractor networks are known to be particularly stable against single-cell fluctuations (Skaggs et al., 1995). Rather, we postulate that the activity bias might be supported by cell-autonomous mechanisms. In the hippocampus, it has been demonstrated that single-cell stimulation can induce a rapid potentiation of synaptic inputs active around the time of stimulation (Bittner et al., 2015). Consistent with this evidence, we speculate that stimulation-evoked spiking in single PreS neurons might have potentiated subthreshold inputs from "visual cells" (Skaggs et al., 1995; Bicanski and Burgess, 2016) active at the stimulus direction. Indeed, computational models have proposed that individual HD neurons might receive inputs from multiple visual feature detector neurons (Skaggs et al., 1995), each of which represents the angular bearing of a particular visual feature of the environment. The weights of these inputs are thought to be modifiable according to a Hebbian rule and thus to critically depend upon postsynaptic spiking: if the postsynaptic HD cell is strongly active, then concomitantly active synapses from visual cells become potentiated (Skaggs et al., 1995; Page et al., 2014; Jeffery et al., 2016). Although our observations are con-

sistent with this hypothesis, intracellular recordings will be required for resolving the underlying synaptic mechanisms (Bittner et al., 2017). We note that the biasing effects described here (Fig. 6) are different from previously reported stimulation effects (Lee et al., 2012; Bittner et al., 2015; Diamantaki et al., 2016; Kim et al., 2017) in that they are weaker (i.e., apparent as a small tuning bias at the population level; Fig. 6) and possibly transient (due to the intrinsic instability of the HD system in the Closed configuration; Fig. 3). We speculate that an enhanced stability of HD signals in the Closed configuration (e.g., by the presentation of behaviorally salient cues) and the possibility of simultaneously activating multiple HD neurons, possibly via the cFos promoter (English et al., 2015) or emerging all-optical approaches (Emiliani et al., 2015; Carillo-Reid et al., 2017; Gauld et al., 2017; Jennings et al., 2017), are likely to result in stronger biasing effects on HD activity.

We provide physiological evidence that, consistent with the known anatomical connectivity (Vogt and Miller, 1983; Thompson and Robertson, 1987; van Groen and Wyss, 1990a,b; Shibata, 1993; Huang et al., 2017), visual inputs can modulate the firing rate of PreS neurons (Fig. 4). A noteworthy observation was that, in our head-fixed preparation, HD activity could not be fully maintained by the presence of a single proximal visual cue (Fig. 3). This finding bears striking similarity to the work of Knierim et al. (1998) finding that, during passive rotations in the dark (but often also in the presence of visual cues), HD firing could become "erratic" and largely uncoupled from the direction of the rat's head. Under passive rotations, only the vestibular system provides information about angular motion; we thus speculate that, in the absence of the normal motor and proprioceptive cues that accompany self-locomotion, angular path integration might be more critically dependent upon (multiple) external landmarks for frequent updates and error corrections. The proximal presentation of the visual cue might have also contributed to the observed instability of the HD representation because animals are known to be less reliant on proximal landmarks even if perceived as stable (Zugaro et al., 2001; Wiener et al., 2002; Yoganarasimha et al., 2006; Knierim and Hamilton, 2011; Yoder et al., 2011). Regardless of the underlying mechanism, and consistent with the interpretation of Knierim et al. (1998), we hypothesize that the degradation of HD signals in the Closed configuration reflects a "disorientated state" of the animal. Enhanced cellular/synaptic plasticity under these conditions (Fig. 6), which could be imposed by neuromodulatory inputs associated with disorientation, would thus ensure an efficient and rapid binding of new landmark inputs arriving onto the PreS HD network.

Despite the reduction in HD tuning strength in the Closed configuration (Fig. 3), we found that cue rotations could gain control of the residual HD signals (Fig. 5). To the best of our knowledge, this is the first evidence indicating that the rapid realignment of HD activity can also be induced in head-fixed animals. Our preparation could thus be useful for future mechanistic studies of HD cell realignment due to its higher mechanical stability (e.g., enabling intracellular recordings) and the precise control over the animal's HD, both of which are difficult to achieve in freely moving animals (Stackman et al., 2003; Lee et al., 2012).

## References


Beed P, Gundlfinger A, Schneiderbauer S, Song J, Böhm C, Burgalossi A, Brecht M, Vida I, Schmitz D (2013) Inhibitory gradient along the dorsoventral axis in the medial entorhinal cortex. Neuron 79:1197–1207. CrossRef Medline

Berens P (2009) CircStat: a MATLAB toolbox for circular statistics. Journal of Statistical Software 31:1–21. CrossRef

Bicanski A, Burgess N (2016) Environmental anchoring of head direction in a computational model of retrosplenial cortex. J Neurosci 36:11601–11618. CrossRef Medline

Bittner KC, Grienberger C, Vaidya SP, Milstein AD, Macklin JJ, Suh J, Tonegawa S, Magee JC (2015) Conjunctive input processing drives feature selectivity in hippocampal CA1 neurons. Nat Neurosci 18:1133–1142. CrossRef Medline

Bittner KC, Milstein AD, Grienberger C, Romani S, Magee JC (2017) Behavioral time scale synaptic plasticity underlies CA1 place fields. Science 357:1033–1036. CrossRef Medline

Blackstad TW (1956) Commissural connections of the hippocampal region in the rat, with special reference to their mode of termination. J Comp Neurol 105:417–537. CrossRef Medline

Boccara CN, Sargolini F, Thoresen VH, Solstad T, Witter MP, Moser EI, Moser MB (2010) Grid cells in pre-and parasubiculum. Nat Neurosci 13:987–994. CrossRef Medline

Burgalossi A, Herfst L, von Heimendahl M, Förste H, Haskic K, Schmidt M, Brecht M (2011) Microcircuits of functionally identified neurons in the rat medial entorhinal cortex. Neuron 70:773–786. CrossRef Medline

Caballero-Bleda M, Witter MP (1993) Regional and laminar organization of projections from the presubiculum and parasubiculum to the entorhinal cortex: an anterograde tracing study in the rat. J Comp Neurol 328:115–129. CrossRef Medline

Caballero-Bleda M, Witter MP (1994) Projections from the presubiculum and the parasubiculum to morphologically characterized entorhinal-hippocampal projection neurons in the rat. Exp Brain Res 101:93–108. Medline

Carillo-Reid L, Han S, Yang W, Yuste R (2017) Modulation of behavioral performance by targeted activation of cortical ensembles in mouse primary visual cortex. Soc Neurosci Abstr 43:147.12.

Cho J, Sharp PE (2001) Head direction, place, and movement correlates for cells in the rat retrosplenial cortex. Behav Neurosci 115:3–25. CrossRef Medline

Christenson MP, Schmidt-Hieber C, Wei H, Hausser M (2016) Cellular mechanisms of sparse coding in hippocampal granule cells. Soc Neurosci Abstr 42:639.24.

Clark BJ, Bassett JP, Wang SS, Taube JS (2010) Impaired head direction cell representation in the anterodorsal thalamus after lesions of the retrosplenial cortex. J Neurosci 30:5289–5302. CrossRef Medline

Diamantaki M, Frey M, Preston-Ferrer P, Burgalossi A (2016) Priming spatial activity by single-cell stimulation in the dentate gyrus of freely moving rats. Curr Biol 26:536–541. CrossRef Medline

Ding SL (2013) Comparative anatomy of the prosubiculum, subiculum, presubiculum, postsubiculum, and parasubiculum in human, monkey, and rodent. J Comp Neurol 521:4145–4162. CrossRef Medline

Doron G, von Heimendahl M, Schlattmann P, Houweling AR, Brecht M (2014) Spiking irregularity and frequency modulate the behavioral report of single-neuron stimulation. Neuron 81:653–663. CrossRef Medline

Dudchenko PA, Goodridge JP, Taube JS (1997) The effects of disorientation on visual landmark control of head direction cell orientation. Exp Brain Res 115:375–380. CrossRef Medline

Emiliani V, Cohen AE, Deisseroth K, Häusser M (2015) All-optical interrogation of neural circuits. J Neurosci 35:13917–13926. CrossRef Medline

English DF, Peyrache A, Kiljan S, Buzsaki G (2015) Functional labeling of restricted populations of head direction neurons in the postsubiculum. Soc Neurosci Abstr 41:257.10.

Gauld OM, Packer AM, Russell LE, Hausser M (2017) Two-photon all-optical interrogation of mouse barrel cortex during a sensory discrimination task. Soc Neurosci Abstr 43:223.09.

Gawne TJ, Kjaer TW, Richmond BJ (1996) Latency: another potential code for feature binding in striate cortex. J Neurophysiol 76:1356–1360. CrossRef Medline

Golob EJ, Taube JS (1999) Head direction cells in rats with hippocampal or overlying neocortical lesions: evidence for impaired angular path integration. J Neurosci 19:7198–7211. Medline

Goodridge JP, Taube JS (1995) Preferential use of the landmark navigational system by head direction cells in rats. Behav Neurosci 109:49–61. CrossRef Medline

Goodridge JP, Taube JS (1997) Interaction between the postsubiculum and

anterior thalamus in the generation of head direction cell activity. J Neurosci 17:9315–9330. Medline
Goodridge JP, Touretzky DS (2000) Modeling attractor deformation in the rodent head direction system. J Neurophysiol 83:3402–3410. CrossRef Medline
Goodridge JP, Dudchenko PA, Worboys KA, Golob EJ, Taube JS (1998) Cue control and head direction cells. Behav Neurosci 112:749–761. CrossRef Medline
Herfst LJ, Brecht M (2008) Whisker movements evoked by stimulation of single motor neurons in the facial nucleus of the rat. J Neurophysiol 99:2821–2832. CrossRef Medline
Herfst L, Burgalossi A, Haskic K, Tukker JJ, Schmidt M, Brecht M (2012) Friction-based stabilization of juxtacellular recordings in freely moving rats. J Neurophysiol 108:697–707. CrossRef Medline
Houweling AR, Brecht M (2008) Behavioural report of single neuron stimulation in somatosensory cortex. Nature 451:65–68. CrossRef Medline
Houweling AR, Doron G, Voigt BC, Herfst LJ, Brecht M (2010) Nanostimulation: manipulation of single neuron activity by juxtacellular current injection. J Neurophysiol 103:1696–1704. CrossRef Medline
Huang LW, Simonnet J, Nassar M, Richevaux L, Lofredi R, Fricker D (2017) Laminar localization and projection-specific properties of presubicular neurons targeting the lateral mammillary nucleus, thalamus, or medial entorhinal cortex. eNeuro 4: pii: ENEURO.0370–0316.2017. CrossRef Medline
Jacob PY, Casali G, Spieser L, Page H, Overington D, Jeffery K (2017) An independent, landmark-dominated head direction signal in dysgranular retrosplenial cortex. Nat Neurosci 20:173–175. CrossRef Medline
Jeffery KJ, Page HJ, Stringer SM (2016) Optimal cue combination and landmark-stability learning in the head direction system. J Physiol 594: 6527–6534. CrossRef Medline
Jennings JH, Kim CK, Marshel J, Raffiee M, Ye L, Quirin S, Pak S, Ramakrishnan C, Deisseroth K (2017) Causal link between neocortical single-cell ensemble activity and specific behaviors. Soc Neurosci Abstr 43:437.06.
Kim SS, Rouault H, Druckmann S, Jayaraman V (2017) Ring attractor dynamics in the *Drosophila* central brain. Science 356:849–853. CrossRef Medline
Klausberger T, Magill PJ, Márton LF, Roberts JD, Cobden PM, Buzsáki G, Somogyi P (2003) Brain-state-and cell-type-specific firing of hippocampal interneurons in vivo. Nature 421:844–848. CrossRef Medline
Knierim JJ, Hamilton DA (2011) Framing spatial cognition: neural representations of proximal and distal frames of reference and their roles in navigation. Physiol Rev 91:1245–1279. CrossRef Medline
Knierim JJ, Kudrimoti HS, McNaughton BL (1995) Place cells, head direction cells, and the learning of landmark stability. J Neurosci 15:1648–1659. Medline
Knierim JJ, Kudrimoti HS, McNaughton BL (1998) Interactions between idiothetic cues and external landmarks in the control of place cells and head direction cells. J Neurophysiol 80:425–446. CrossRef Medline
Knight R, Piette CE, Page H, Walters D, Marozzi E, Nardini M, Stringer S, Jeffery KJ (2014) Weighted cue integration in the rodent head direction system. Philos Trans R Soc Lond B Biol Sci 369:20120512. CrossRef Medline
Lee D, Lin BJ, Lee AK (2012) Hippocampal place fields emerge upon single-cell manipulation of excitability during behavior. Science 337:849–853. CrossRef Medline
McNaughton BL, Chen LL, Markus EJ (1991) "Dead reckoning," landmark learning, and the sense of direction: a neurophysiological and computational hypothesis. J Cogn Neurosci 3:190–202. CrossRef Medline
Naumann RK, Anjum F, Roth-Alpermann C, Brecht M (2012) Cytoarchitecture, areas, and neuron numbers of the etruscan shrew cortex. J Comp Neurol 520:2512–2530. CrossRef Medline
Page HJ, Walters DM, Knight R, Piette CE, Jeffery KJ, Stringer SM (2014) A theoretical account of cue averaging in the rodent head direction system. Philos Trans R Soc Lond B Biol Sci 369:20130283. CrossRef Medline
Pérez-Escobar JA, Kornienko O, Latuske P, Kohler L, Allen K (2016) Visual landmarks sharpen grid cell metric and confer context specificity to neurons of the medial entorhinal cortex. Elife 5:e16937. CrossRef Medline
Pinault D (1994) Golgi-like labeling of a single neuron recorded extracellularly. Neurosci Lett 170:255–260. CrossRef Medline
Pinault D (1996) A novel single-cell staining procedure performed in vivo under electrophysiological control: morpho-functional features of juxtacellularly labeled thalamic cells and other central neurons with biocytin or neurobiotin. J Neurosci Methods 65:113–136. CrossRef Medline
Preston-Ferrer P, Coletta S, Frey M, Burgalossi A (2016) Anatomical organization of presubicular head direction circuits. eLife 5:e14592. CrossRef Medline
Quilichini P, Sirota A, Buzsáki G (2010) Intrinsic circuit organization and theta–gamma oscillation dynamics in the entorhinal cortex of the rat. J Neurosci 30:11128–11142. CrossRef Medline
Ray S, Naumann R, Burgalossi A, Tang Q, Schmidt H, Brecht M (2014) Grid-layout and theta-modulation of layer 2 pyramidal neurons in medial entorhinal cortex. Science 343:891–896. CrossRef Medline
Redish AD, Elga AN, Touretzky DS (1996) A coupled attractor model of the rodent head direction system. Network: Computation in Neural Systems 7:671–685. CrossRef
Seelig JD, Jayaraman V (2015) Neural dynamics for landmark orientation and angular path integration. Nature 521:186–191. CrossRef Medline
Sharp PE, Blair HT, Brown M (1996) Neural network modeling of the hippocampal formation spatial signals and their possible role in navigation: a modular approach. Hippocampus 6:720–734. CrossRef Medline
Shibata H (1993) Direct projections from the anterior thalamic nuclei to the retrohippocampal region in the rat. J Comp Neurol 337:431–445. CrossRef Medline
Simonnet J, Nassar M, Stella F, Cohen I, Mathon B, Boccara CN, Miles R, Fricker D (2017) How activity dependent feedback inhibition may maintain head direction signals in mouse presubiculum. Nat Commun 8:16032. CrossRef Medline
Skaggs WE, Knierim JJ, Kudrimoti HS, McNaughton BL (1995) A model of the neural basis of the rat's sense of direction. Adv Neural Inf Process Syst 7:173–180. Medline
Song P, Wang XJ (2005) Angular path integration by moving "hill of activity": a spiking neuron model without recurrent excitation of the head direction system. J Neurosci 25:1002–1014. CrossRef Medline
Stackman RW, Golob EJ, Bassett JP, Taube JS (2003) Passive transport disrupts directional path integration by rat head direction cells. J Neurophysiol 90:2862–2874. CrossRef Medline
Tang Q, Brecht M, Burgalossi A (2014) Juxtacellular recording and morphological identification of single neurons in freely moving rats. Nat Protoc 9:2369–2381. CrossRef Medline
Taube JS (1995a) Place cells recorded in the parasubiculum of freely moving rats. Hippocampus 5:569–583. CrossRef Medline
Taube JS (1995b) Head direction cells recorded in the anterior thalamic nuclei of freely moving rats. J Neurosci 15:70–86. Medline
Taube JS (2007) The head direction signal: origins and sensory-motor integration. Annu Rev Neurosci 30:181–207. CrossRef Medline
Taube JS, Bassett JP (2003) Persistent neural activity in head direction cells. Cereb Cortex 13:1162–1172. CrossRef Medline
Taube JS, Burton HL (1995) Head direction cell activity monitored in a novel environment and during a cue conflict situation. J Neurophysiol 74:1953–1971. CrossRef Medline
Taube JS, Muller RU, Ranck JB Jr (1990a) Head direction cells recorded from the postsubiculum in freely moving rats. II. Effects of environmental manipulations. J Neurosci 10:436–447. Medline
Taube JS, Muller RU, Ranck JB Jr (1990b) Head direction cells recorded from the postsubiculum in freely moving rats. I. Description and quantitative analysis. J Neurosci 10:420–435. Medline
Thompson SM, Robertson RT (1987) Organisation of subcortical pathways for sensory projections to the limbic cortex. I. Subcortical projections to the medial limbic cortex in the rat. J Comp Neurol 265:175–188. CrossRef Medline
Tukker JJ, Tang Q, Burgalossi A, Brecht M (2015) Head directional tuning and theta modulation of anatomically identified neurons in the presubiculum. J Neurosci 35:15391–15395. CrossRef Medline
van Groen T, Wyss JM (1990a) Connections of the retrosplenial granular a cortex in the rat. J Comp Neurol 300:593–606. CrossRef Medline
van Groen T, Wyss JM (1990b) The postsubicular cortex in the rat: characterization of the fourth region of the subicular cortex and its connections. Brain Res 529:165–177. CrossRef Medline
Vogt BA, Miller MW (1983) Cortical connections between rat cingulate cortex and visual, motor, and postsubicular cortices. J Comp Neurol 216: 192–210. CrossRef Medline

Wiener SI, Berthoz A, Zugaro MB (2002) Multisensory processing in the elaboration of place and head direction responses by limbic system neurons. Brain Res Cogn Brain Res 14:75–90. CrossRef Medline

Wolff T, Iyer NA, Rubin GM (2015) Neuroarchitecture and neuroanatomy of the *Drosophila* central complex: a GAL4-based dissection of protocerebral bridge neurons and circuits. J Comp Neurol 523:997–1037. CrossRef Medline

Yoder RM, Taube JS (2014) The vestibular contribution to the head direction signal and navigation. Front Integr Neurosci 8:32. CrossRef Medline

Yoder RM, Clark BJ, Taube JS (2011) Origins of landmark encoding in the brain. Trends Neurosci 34:561–571. CrossRef Medline

Yoganarasimha D, Yu X, Knierim JJ (2006) Head direction cell representations maintain internal coherence during conflicting proximal and distal cue rotations: comparison with hippocampal place cells. J Neurosci 26:622–631. CrossRef Medline

Zhang K (1996) Representation of spatial orientation by the intrinsic dynamics of the head direction cell ensemble: a theory. J Neurosci 16:2112–2126. Medline

Zugaro MB, Tabuchi E, Wiener SI (2000) Influence of conflicting visual, inertial and substratal cues on head direction cell activity. Exp Brain Res 133:198–208. CrossRef Medline

Zugaro MB, Berthoz A, Wiener SI (2001) Background, but not foreground, spatial cues are taken as references for head direction responses by rat anterodorsal thalamus neurons. J Neurosci 21:RC154. Medline

Zugaro MB, Arleo A, Berthoz A, Wiener SI (2003) Rapid spatial reorientation and head direction cells. J Neurosci 23:3478–3482. Medline